JOURNAL OF PETROLOGY | VOLUME 51 | NUMBER 12 | PAGES 2445–2464 | 2010 | doi:10.1093/petrology/egq063

The Magnetite Crisis in the Evolution of Arc-related Magmas and the Initial Concentration of Au, Ag and Cu

FRANCES E. JENNER[1]†*, HUGH ST. C. O'NEILL[1], RICHARD J. ARCULUS[1] AND JOHN A. MAVROGENES[1]

[1]RESEARCH SCHOOL OF EARTH SCIENCES, AUSTRALIAN NATIONAL UNIVERSITY, CANBERRA, ACT 0200, AUSTRALIA

RECEIVED FEBRUARY 2, 2010; ACCEPTED SEPTEMBER 16, 2010

The association of large Au–Cu–Ag ore deposits with convergent margins is commonly attributed to the higher content of chalcophile elements in the parental magmas generated at subduction zones compared with mid-ocean ridges. We present new geochemical data for arc-like, relatively oxidized mantle-derived basalt to rhyolite magmas from the Pual Ridge and vicinity, Eastern Manus Basin, which show that the initial abundances of base and precious metals in the parental basalts are similar to those of mid-ocean ridge basalt (MORB). The contents of Au, Cu, and Ag are built up in the evolving Pual Ridge liquids to levels considerably in excess of those in MORB because, unlike MORB, they are not saturated in a sulfide phase, which is a consequence of their being more oxidized than MORB. The behaviour of S during the evolution of the Pual Ridge magmas is obscured by late-stage SO_2 loss during eruption, but we show that it may be inferred by using Se as a proxy, because this element follows S closely during magmatic evolution except it is not lost during low-pressure (near sea-floor) degassing. The onset of magnetite fractionation at ~60 wt % SiO_2 and an Mg-number of ~40 is accompanied by an abrupt decrease in the contents of Au, Cu and Ag, previously attributed to separation of Cu–Au-rich fluid, which is also shown by Se, implying that magnetite fractionation triggers sulfide saturation. Petrological modelling reveals that the amount of magnetite fractionation involved is sufficient to convert most of the S originally dissolved in the magma as sulfate (SO_4^{2-}) to sulfide (S^{2-}), triggering saturation in a Cu-rich sulfide phase, tentatively identified as bornite (Cu_5FeS_4). This sulfide phase sequesters Au and Ag, elements with the same valence as Cu in sulfides, but not other potentially chalcophile elements such as Ni, Re, and Pt, which suggests that the phase is crystalline rather than an immiscible sulfide melt. The relatively high contents of Cu and Au characteristic of evolved convergent margin magmas requires no enrichment from subducted material. Instead, the association of major Cu–Au deposits with convergent-margin magmatism results specifically from the process of magmatic evolution under oxidizing conditions. This same property also leads to early magnetite fractionation, triggering the abrupt saturation in the Cu-rich sulfide. Hence the easily recognizable trend of magmatic evolution under oxidizing conditions (i.e. the sharp drop in chalcophile element concentrations) may be an exploration guide to economic Au–Ag–Cu provinces, or a crucial pre-enrichment step in the formation of such deposits. The decrease in P_2O_5 and Sr at the same stage in the fractionation sequence (~60 wt % SiO_2) indicates that saturation in apatite is concomitant with magnetite–sulfide saturation in the Eastern Manus Basin.

KEY WORDS: *selenium; sulfide; magnetite; chalcophile; subduction*

INTRODUCTION

One conspicuous feature of arc and back-arc magma series is their association with ores of the rare, but economically important metals Au, Cu, and Ag. Understanding the geological processes leading to the selective concentration of these metals is not straightforward. For Au, one of the rarest metals on Earth, with a primitive mantle abundance of only 0·9 ppb (Palme & O'Neill, 2003), enrichments by a factor of 10^3 are needed to form economically attractive

*Corresponding author: Telephone: (+81) 0858-43-3823.
E-mail: frances@misasa.okayama-u.ac.jp
†Present address: The Pheasant Memorial Laboratory for Geochemistry and Cosmochemistry (PML), Institute for Study of the Earth's Interior, Okayama University at Misasa, Misasa, Tottori-ken 682-0193, Japan.

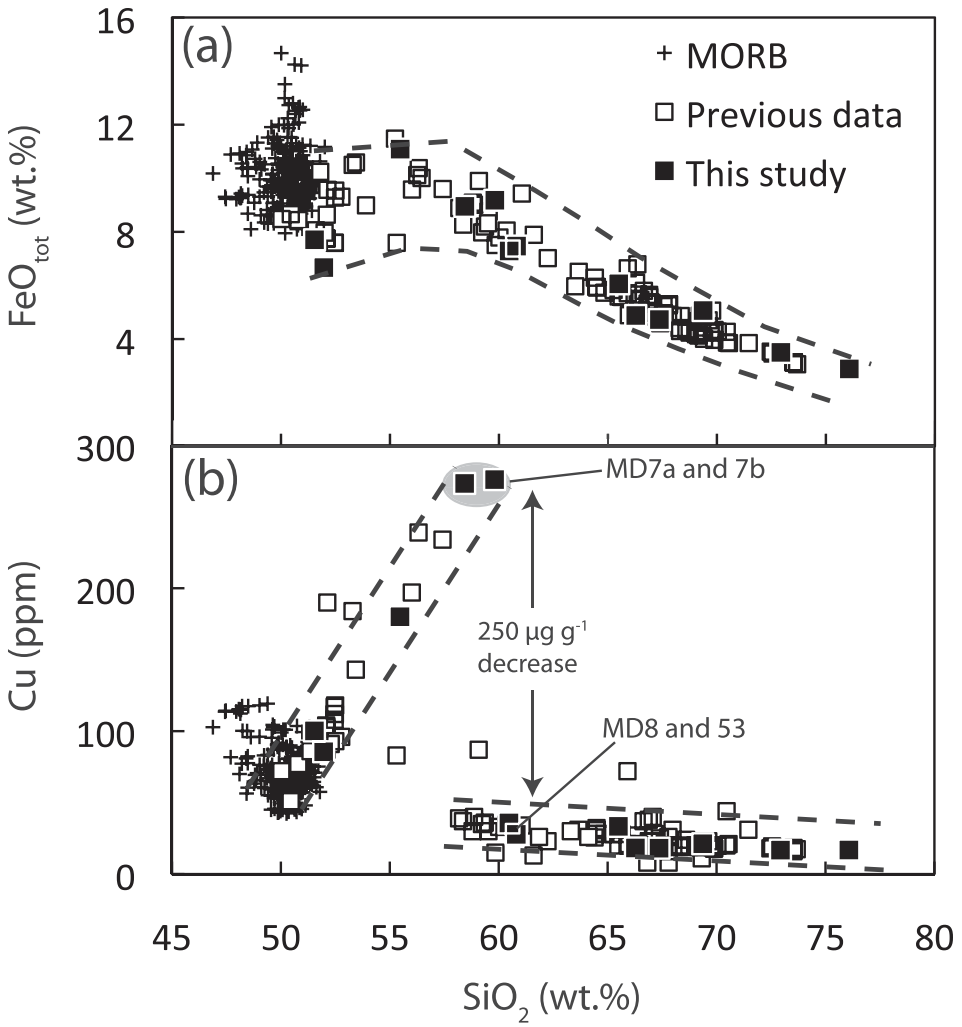

Fig. 1. Covariation of (a) FeO_{tot} and (b) Cu vs SiO_2 for samples from the Pual Ridge, Eastern Manus Basin, demonstrating the sudden drop in Cu contents at ~60 wt % SiO_2, which coincides with the change in FeO_{tot} partitioning behaviour. Analyses from this study encompass the range in compositions of the previous studies of Kamenetsky *et al.* (2001), Moss & Scott (2001), Sun *et al.* (2004) and Park *et al.* (2010).

ores. How this happens is particularly perplexing for Au, because this egregiously inert metal does not appear to be incompatible during crust–mantle differentiation. Compared with either the primitive mantle or mid-ocean ridge basalts (MORBs; which typically contain ~1·2 ppb Au; Supplementary Data Table 1, available at http://petrology.oxfordjournals.org/), the content of Au in the continental crust is only ~1·5 ppb (Rudnick & Gao, 2008).

Although the spatial relationship between Au–Cu-rich sulfide deposits and convergent margin magmatism is well established (e.g. Hedenquist & Lowenstern, 1994), the reason for this association is unclear. Studies of Au ores themselves have given few clues to the earliest stages of the enrichment process. A significant discovery of Moss & Scott (2001) and Sun *et al.* (2004) was that a trend of increasing Cu and Au with SiO_2 in evolving arc-like magmas of the Pual Ridge and vicinity (Eastern Manus region of the Manus back-arc basin) is suddenly interrupted at ~60 wt % SiO_2 (Fig. 1). The low Cu and Au contents in the most evolved samples from the Manus area have been attributed to loss in a fugitive volatile phase (e.g. Loucks & Mavrogenes, 1999), possibly triggered by magnetite saturation and accompanying redox changes in an evolving crustal magma chamber (Binns & Scott, 1993; Kamenetsky *et al.*, 2001; Moss & Scott, 2001; Sun *et al.*, 2004).

Arc-related volcanic rocks from the Pual Ridge area range in composition from basalt to rhyolite, forming a typical example of magmatic evolution by fractional crystallization (Binns & Scott, 1993; Kamenetsky *et al.*, 2001;

Moss & Scott, 2001; Sinton *et al.*, 2003; Sun *et al.*, 2003, 2004, 2007; Park *et al.*, 2010). We have re-analysed the Pual Ridge sample set at intervals along the range in SiO_2 and Cu contents (Fig. 1) for a more comprehensive list of trace elements, including the key element Se, which proxies the behaviour of S during magmatic evolution without being affected by volatile loss upon quenching. It would be helpful in understanding the behaviour of chalcophile elements in arc-related lavas to contrast their behaviour with that during basaltic magma evolution in other tectonic settings, the best understood of which is mid-ocean ridge magmatism. However, data for chalcophile element contents in MORBs in the literature are meagre, in particular for Ag and Se. Accordingly, we present 252 new analyses of volcanic glasses (loaned from the Department of Mineral Sciences, US National Museum of Natural History, Washington, DC) from ocean-floor basalts (ridges but also associated fracture zones, referred to collectively as MORB throughout this paper for ease of reference) from the Pacific and Atlantic Oceans. Comparison of these new analyses of a global range of MORB with the Pual Ridge volcanic glasses shows that, contrary to previous hypotheses (e.g. Mungall, 2002), no enrichment of these ore-forming metals from slab-derived inputs into the mantle wedge source of arc magmas is required, as previously suggested by Hamlyn *et al.* (1985). Additionally, we demonstrate that the behaviour of Cu and Au following magnetite fractionation is paralleled by Ag and importantly Se, indicating that saturation in a sulfide phase is responsible for the sudden drop in chalcophile element abundances as opposed to the separation of a chalcophile-rich fluid or vapour phase.

ANALYTICAL METHODS

Major and minor (S, Cl) element analyses of Pual Ridge glasses were obtained at the Australian National University using a Cameca SX100 electron microprobe following the methods described by O'Neill & Mavrogenes (2002). Trace element abundances were determined by laser ablation–inductively coupled plasma mass spectrometry (LA-ICP-MS) using a 7500S Agilent system (RF power 1300 W; ablation cell gas flow 0·3 l min^{-1} He, 0·02 l min^{-1} H_2; auxiliary gas flow 1·0 l min^{-1} Ar; laser energy 50–55 mJ), coupled to an ANU HelEX laser ablation system, which employs a 193 nm wavelength EXCIMER laser [110 (ArF) COMPex, Lambda Physik]. Analysis of Se followed methods described by Jenner *et al.* (2009). Data acquisition for elements other than Au, Re and Pt was performed with 20 s of background measurement, followed by 40 s of sample ablation, an ablation diameter of 86 μm and a repetition rate of 5 Hz (with the exception Ag, Cd and In analyses, where a repetition rate of 10 Hz was employed to achieve more sensitive analytical conditions). To achieve the lower limits of detection required for Au, Pt and Re analyses, longer counting times were used (30 s of background measurement, followed by 50 s of sample ablation), and a larger ablation diameter of 187 μm and a repetition rate of 10 Hz were employed. To minimize the potential for oxide production, the LA-ICP-MS system was calibrated to low oxide production rates (ThO^+/Th^+ typically <0·4%) and this rate was monitored throughout each analytical session. Additionally, a range of experimental, high-REE (rare earth element) glasses (Evans *et al.*, 2008*b*), zircon and rutile were used to measure isotopic interferences on a range of masses throughout data collection (e.g. oxide production rates; $^{91}Zr^{16}O$, $^{169}Tm^{16}O$, $^{179}Hf^{16}O$ and $^{181}Ta^{16}O$ production rate on ^{107}Ag, ^{185}Re, ^{195}Pt and ^{197}Au, respectively; and doubly charged REE production rates such as $^{150}Nd^{2+}$ and $^{150}Sm^{2+}$ on ^{75}As), permitting precise interference corrections [following methods described by Hu *et al.* (2009) and Jenner *et al.* (2009)].

All samples and standards were analysed in batches of ~12, with NIST SRM 612 (values given in Table 1) used for external calibration, analysed at the beginning and end of each batch to allow corrections to be made for instrument drift. The discrete compositional rods within each of the NIST SRM glasses described by Eggins & Shelley (2002) were avoided. The abundances of SiO_2 from the electron microprobe analyses were used for internal calibration, with a correction factor of 1·063 to account for the differences in ablation characteristics between NIST SMR 612 and the natural volcanic glasses (e.g. Gaboardi & Humayun, 2009). Data reduction was performed using the method described by Longerich *et al.* (1996).

Data for replicate analyses of NIST SRM 614 are listed in Table 1 along with the range in values for each element from the GeoReM website (Jochum & Stoll, 2008). The percentage relative standard deviations (% RSDs) for replicate analyses of NIST SRM 614 are all ≤4·9% and typically ~2%, demonstrating the precision of the LA-ICP-MS technique. In particular, replicate analyses of Re, Pt and Au show 1·67, 0·66 and 2·03% RSD, respectively. Analyses of the Pual Ridge suite and MORB samples are given in Table 1 and Supplementary Data Table 1, respectively.

CHALCOPHILE ELEMENT SYSTEMATICS OF MORB

The abundance of S and chalcophile elements (i.e. Au, Cu, Ag, and Se) in relatively reduced basaltic melts such as MORB is controlled by saturation with Fe–Ni-rich sulfide (Mathez, 1976; Czamanske & Moore, 1977; Hertogen *et al.*, 1980; Peach *et al.*, 1990; Yi *et al.*, 2003). During fractional crystallization, Cu is highly compatible in sulfide, and

Table 1: List of values for NIST SRM 612 used for external calibration of LA-ICP-MS data, major and trace element analyses of volcanic glasses from the Pual Ridge, and analyses of NIST SRM 614 compared with the GeoReM range

	NIST SRM 612		Pual Ridge, Manus Basin, SW Pacific													NIST SRM 614 ($n = 10$)		
	PV	Ref.	MD3	MD101	DR86	MD7A	MD76	MD8	MD53	MD65	MD28	MD36	MD114	DR87	MD6	Average	RSD (%)	GeoReM
wt %																		
SiO_2			51·96	51·54	55·47	58·44	59·81	60·81	60·47	67·36	66·28	69·37	65·49	72·93	76·07			
Al_2O_3			12·99	15·34	14·93	15·32	14·93	15·62	15·69	14·77	14·59	14·35	14·45	12·84	11·86			
FeO_{tot}			6·67	7·71	11·09	8·95	9·18	7·47	7·29	4·73	4·88	5·06	6·06	3·50	2·89			
MgO			9·19	6·86	4·24	3·22	3·07	2·39	2·43	1·50	1·41	1·04	1·13	0·26	0·15			
CaO			14·37	11·81	8·09	7·15	6·79	5·84	5·89	3·65	3·56	3·41	3·58	1·79	1·11			
Na_2O			1·59	1·89	3·11	3·59	3·77	4·16	4·08	4·59	4·51	4·68	4·75	4·73	4·58			
K_2O			0·25	0·32	0·68	0·84	0·92	1·08	1·07	1·56	1·57	1·55	1·34	1·69	2·49			
TiO_2			0·38	0·45	0·83	1·17	1·23	1·06	1·06	0·70	0·67	0·66	0·76	0·43	0·35			
P_2O_5			0·09	0·18	0·35	0·67	0·81	0·63	0·43	0·20	0·21	0·28	0·39	0·15	0·05			
MnO			0·13	0·16	0·18	0·19	0·21	0·17	0·17	0·15	0·14	0·15	0·15	0·11	0·09			
Total			97·61	96·26	98·95	99·55	100·72	99·23	98·57	99·19	97·81	100·55	98·11	98·45	99·65			
ppm																		
S			12	11	14	16	13	15	26	6	5	10	6	3	148			
Cl			81	65	205	183	197	221	210	290	301	318	309	510	499			
Li	42	1	4·86	5·35	7·70	7·49	8·17	10·31	9·17	13·89	14·64	15·90	15·94	16·10	16·23	1·496	2·42	1·44–1·95
Be	38	1	0·24	0·27	0·65	0·62	0·79	0·91	0·78	1·16	1·12	1·30	1·19	1·24	1·49	0·729	0·73	0·4–0·79
Sc	39	2	40·68	37·92	34·36	27·08	25·17	23·47	24·39	16·52	16·59	15·20	16·84	11·27	9·97	1·602	0·85	0·89–5·55
Ti	41	2	2849	2906	5502	6450	7139	7017	6519	4729	4651	5212	5510	3025	2416	2·870	2·31	2·42–3·77
V	39	1	279·9	287·7	476·2	413·2	458·6	201·8	263·7	41·92	41·87	40·21	60·47	4·08	2·66	0·947	0·97	0·87–1·12
Cr	39·9	3	183·8	138·5	17·06	0·91	0·78	17·64	1·91	34·95	30·60	1·21	2·88	0·59	0·63	1·353	4·86	0·99–10·7
Mn	38	1	1318	1310	1436	1335	1331	1406	1338	1143	1188	1203	1278	960	807	1·303	0·49	0·692–2·2
Co	35	1	44·37	40·20	35·64	26·26	25·76	16·96	18·98	8·23	8·36	7·46	8·78	2·47	2·49	0·693	0·55	0·63–2·32
Ni	38·8	1	70·76	66·05	23·71	6·17	5·92	8·65	2·01	19·04	17·17	2·82	3·64	0·290	0·211	0·996	2·25	0·9–6·1
Cu	37	1	85·59	100·18	180·07	273·32	276·02	27·77	35·78	18·11	18·26	21·22	33·39	16·76	16·84	1·185	1·05	1·19–4·41
Zn	38	1	78·7	77·4	96·4	96·7	106·4	118·0	102·6	102·5	101·4	110·0	113·0	79·2	82·6	2·197	1·30	1·76–3·68
As (i)	37	1	1·383	1·316	1·772	1·599	2·109	2·476	2·355	3·411	3·293	3·557	3·200	3·994	4·542	1·144	3·75	0·593–0·72
Se (i)	15·2	4	0·119	0·139	0·247	0·348	0·355	0·143	0·158	0·137	0·146	0·158	0·177	0·153	0·137	0·394	3·05	n.a.
Rb	31·4	1	3·80	5·48	12·44	11·42	14·80	17·01	15·71	26·45	24·80	30·40	25·53	32·84	36·55	0·792	2·00	0·73–0·98
Sr	78·4	1	245	240	436	567	475	426	436	301	292	339	329	215	221	43·55	0·70	42·4–48·58
Y	38	1	10·06	11·29	19·73	17·30	23·90	29·79	25·21	30·44	30·59	32·42	33·39	34·87	36·19	0·727	1·42	0·7–1
Zr	38	1	23·19	25·40	53·99	49·25	67·98	80·89	69·01	113·9	110·5	122·1	117·8	151·1	158·4	0·800	1·53	0·77–0·95
Nb	40	1	0·35	0·32	0·84	0·88	1·14	1·30	1·14	1·88	1·78	1·99	1·91	2·38	2·31	0·827	0·75	0·68–0·89
Ag (i)	21·4	5	0·04	0·03	0·06	0·08	0·08	0·02	0·02	0·02	0·02	0·03	0·03	0·03	0·03	0·40	1·49	0·361

(continued)

Table 1: Continued

	NIST SRM 612		Pual Ridge, Manus Basin, SW Pacific												NIST SRM 614 ($n = 10$)		
	PV	Ref.	MD3	MD101	DR86	MD7A	MD76	MD8	MD53	MD65	MD28	MD36	MD114	DR87	MD6	Average	RSD (%)	GeoReM
Cd	28·3	5	0·13	0·13	0·14	0·12	0·16	0·15	0·14	0·15	0·16	0·17	0·18	0·12	0·13	0·488	1·51	0·566–0·64
In (i)	37	5	0·04	0·04	0·06	0·05	0·07	0·06	0·06	0·07	0·07	0·07	0·08	0·06	0·06	0·804	0·99	0·73–1·2
Sn	35·6	5	0·31	0·30	0·52	0·55	0·59	0·69	0·62	0·95	0·97	1·05	1·02	1·00	1·20	1·445	1·14	1·4–1·78
Sb	31·4	5	0·03	0·03	0·05	0·05	0·06	0·07	0·07	0·10	0·10	0·09	0·09	0·12	0·14	0·720	2·30	0·69–0·86
Cs	42	1	0·16	0·18	0·33	0·29	0·40	0·48	0·43	0·69	0·67	0·76	0·68	0·86	0·90	0·601	0·81	0·59–0·76
Ba	39·7	1	80·5	86·6	176·7	164·8	227·6	259·2	220·1	356·1	334·3	390·3	346·2	430·1	460·0	2·826	1·17	2·9–3·44
La	35·8	1	1·88	2·23	5·70	5·63	7·66	8·72	7·28	10·31	9·95	11·61	10·98	12·12	13·15	0·665	1·89	0·68–0·78
Ce	38·7	1	5·03	5·62	13·52	13·40	18·30	20·78	17·77	24·17	23·91	27·22	26·16	28·35	30·90	0·752	1·38	0·735–1·04
Pr	38·95	TS	0·78	0·83	2·00	2·01	2·79	3·10	2·61	3·47	3·36	3·87	3·65	3·99	4·33	0·737	0·89	0·7–0·8
Nd	35·9	1	3·85	4·29	9·74	9·59	13·37	15·44	12·65	15·95	15·90	17·80	17·52	17·76	19·13	0·700	3·05	0·699–0·78
Sm	38·1	1	1·20	1·32	2·79	2·58	3·59	4·29	3·63	4·14	4·17	4·71	4·74	4·79	4·93	0·719	2·35	0·7–0·81
Eu	35	1	0·46	0·50	1·00	0·98	1·27	1·40	1·20	1·27	1·20	1·38	1·44	1·19	1·29	0·714	1·16	0·72–0·8
Gd	36·7	1	1·48	1·63	3·05	2·92	3·92	4·68	3·85	4·29	4·44	4·98	4·88	5·00	5·18	0·701	2·47	0·68–0·82
Tb	38·3	TS	0·25	0·29	0·53	0·48	0·67	0·80	0·66	0·75	0·78	0·85	0·85	0·87	0·90	0·701	1·86	0·67–0·77
Dy	36	1	1·85	2·07	3·39	3·04	4·35	5·28	4·25	5·02	5·05	5·86	5·65	5·83	6·13	0·698	1·44	0·68–0·83
Ho	38	1	0·40	0·44	0·74	0·66	0·89	1·12	0·88	1·11	1·05	1·19	1·19	1·26	1·29	0·680	1·39	0·7–0·81
Er	38	1	1·16	1·32	2·24	2·00	2·70	3·31	2·67	3·31	3·32	3·73	3·66	3·88	4·01	0·695	1·54	0·65–0·81
Tm	38	1	0·17	0·19	0·33	0·30	0·39	0·49	0·40	0·51	0·50	0·55	0·56	0·61	0·63	0·665	1·17	0·67–0·8
Yb	37·1	TS	1·11	1·29	2·12	1·86	2·55	3·09	2·65	3·36	3·37	3·78	3·68	3·96	4·16	0·657	1·93	0·7–1
Lu	37·18	6	0·18	0·20	0·33	0·29	0·40	0·48	0·42	0·54	0·54	0·59	0·58	0·66	0·69	0·657	1·09	0·67–0·8
Hf	37·9	6	0·73	0·80	1·68	1·47	1·95	2·49	2·12	3·28	3·22	3·58	3·62	4·31	4·62	0·648	1·66	0·6–0·77
Ta	40	1	0·02	0·02	0·05	0·05	0·08	0·08	0·07	0·11	0·10	0·12	0·11	0·14	0·15	0·745	1·11	0·7–0·86
W	38·08	6	0·03	0·03	0·06	0·08	0·08	0·11	0·09	0·14	0·15	0·18	0·14	0·19	0·22	0·741	1·39	0·74–1·2
Re* (i)	6·57	7	1·31	1·01	1·21	1·45	1·98	1·84	1·94	0·60	0·69	0·82	1·04	0·37	0·15	156	1·67	155–179
Pt* (i)	2·59	7	6·10	4·22	1·93	3·62	2·44	1·51	1·99	0·84	0·26	0·95	1·15	b.d.l.	1·00	2370	0·66	2260–2400
Au* (i)	4·58	7	3·63	3·55	5·28	5·81	6·78	1·10	1·33	0·63	0·79	0·69	1·00	b.d.l.	0·81	443	2·03	410–519
Tl	15·1	1	0·04	0·05	0·09	0·09	0·11	0·13	0·12	0·19	0·20	0·23	0·20	0·23	0·26	0·238	1·98	0·24–0·3
Pb	38·57	1	1·24	1·37	2·50	2·47	3·07	3·71	3·26	5·06	4·86	5·53	4·99	5·44	6·38	2·118	1·46	1·95–2·83
Bi	30	1	0·02	0·01	0·02	0·03	0·04	0·03	0·03	0·05	0·05	0·05	0·04	0·05	0·05	0·521	1·02	0·5–0·68
Th	37·79	1	0·17	0·26	0·49	0·48	0·63	0·81	0·67	1·21	1·16	1·32	1·23	1·50	1·66	0·683	1·55	0·71–1·2
U	37·38	1	0·11	0·12	0·33	0·29	0·37	0·43	0·43	0·64	0·70	0·79	0·77	0·94	1·11	0·748	1·52	0·78–1·06

Data sources for NIST SRM 612 values: (1) Jochum & Stoll (2008); (2) Eggins (2003); (3) Humayun *et al.* (2007); (4) Jenner *et al.* (2009); (5) Hu *et al.* (2009), (6) Nebel *et al.* (2009); (7) Sylvester & Eggins (1997). Locations and sample descriptions for Pual Ridge glasses have been given by Sun *et al.* (2004) and references therein. GeoReM range as updated by Jochum & Stoll (2008). Ref., reference for NIST SRM 612 value; TS (this study), F. E. Jenner & H. S. C. O'Neill (unpublished data); (i), interference corrected; b.d.l., below detection limit (detection limits for Au, Re and Pt typically >0·25 ppb (following interference corrections); RSD, relative standard deviation; n.a., no available data; PV, preferred value.
*Values in ppb.

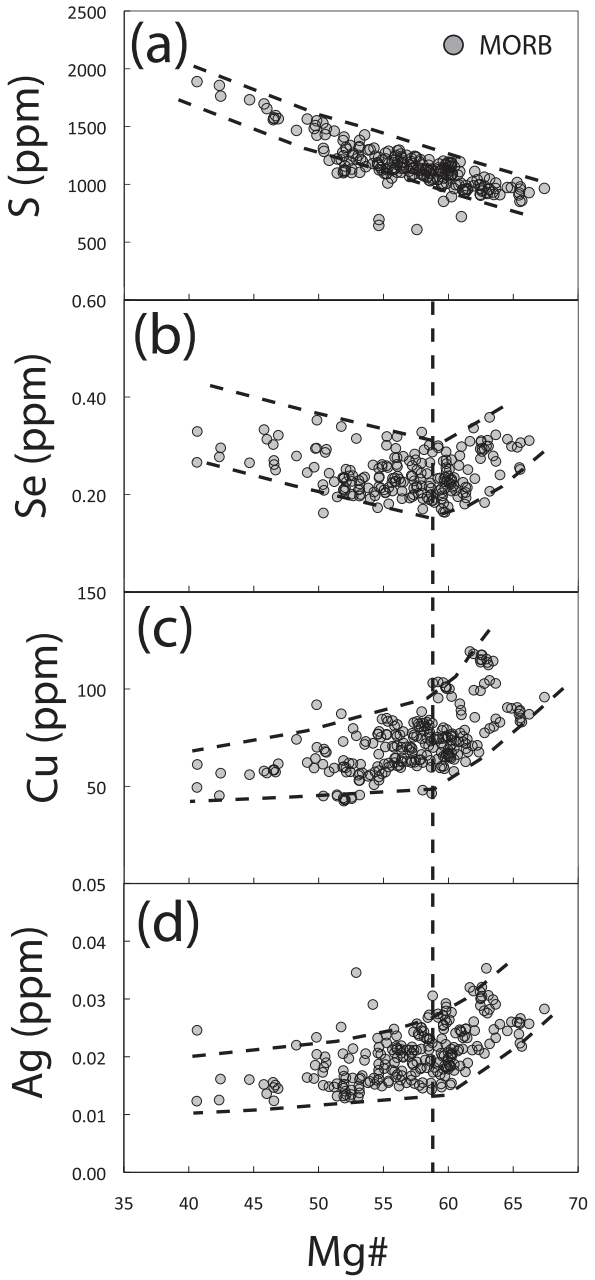

Fig. 2. Covariation diagrams showing variations in (a) S, (b) Se, (c) Cu, and (d) Ag vs Mg-number for mid-ocean ridge and fracture zone basalts, collectively referred to in the text as MORB.

its content in MORB melts decreases with continued fractional crystallization (e.g. Czamanske & Moore, 1977; Doe, 1994, 1995). Few analyses are available in the literature for Se and Ag contents in mantle-derived rocks, which has limited our current understanding of their behaviour during differentiation of a cooling magma. The MORB samples from the Pacific and Atlantic analysed as part of this study show a steady increase in S with decreasing Mg-number (Fig. 2), where Mg-number = molar Mg/(Mg + Fe) × 100, a more sensitive measure of magmatic evolution in MORB than SiO_2, which changes little during crystallization of cotectic olivine + plagioclase + clinopyroxene in the low-pressure evolution of these magmas, as noted above. Because FeO increases under the reduced, relatively anhydrous conditions prevailing during MORB fractionation, S content also increases, despite concurrent fractionation of sulfide, because the S content at sulfide saturation of a silicate melt is primarily a function of its FeO content (e.g. O'Neill & Mavrogenes, 2002).

In MORB, Se, Cu, and Ag initially decrease with decreasing Mg-number (Fig. 2), which is attributable to the removal of these elements in a sulfide phase during fractional crystallization. The decreases in Cu/S, Se/S and Cu/Se and the relatively constant Cu/Ag (average of 3552 ± 364) with decreasing Mg-number in MORB (Fig. 3) indicate compatibility in magmatic sulfide that increases in the order Cu ≈ Ag > Se > S during low-pressure differentiation. The higher compatibility of Cu relative to Se in magmatic sulfides is contrary to the previous appraisal of the partitioning behaviour of chalcophile elements in MORB (Peach *et al.*, 1990), but is consistent with the chalcophile element partitioning behaviour during removal of sulfide liquid from the fractionating magma of the Bushveld Complex, South Africa, documented by Barnes *et al.* (2009).

CHALCOPHILE ELEMENT SYSTEMATICS OF MANUS BACK-ARC BASIN MAGMAS

The most primitive samples from the Pual Ridge (highest Mg-number and lowest SiO_2) have V, Co, Pt, Re, Cu, Ag and Au contents comparable with those in primitive MORB (Figs 4 and 5), demonstrating that the mantle wedge was not enriched in these elements. In contrast, the abundances of FeO_{tot}, TiO_2, and Se are lower than those in MORB at a similar Mg-number. The abundances of Pt and Co decrease with decreasing Mg-number, indicating that these elements are partitioned into olivine, chromite, and/or clinopyroxene early in the fractionation sequence (Fig. 4). The fractionating crystalline assemblage forces the contents of FeO_{tot}, V, Re, TiO_2, P_2O_5 and Sr to initially increase (Fig. 4). It is worth noting that there are major differences in the crystallization sequences of relatively wet basalts from arc or back-arc environments compared with dry magmas such as MORBs (Arculus, 2004). Basalts in both tectonic situations are saturated initially with olivine and Cr-rich spinel, but the next phase to appear at low pressures is generally plagioclase in the dry magmas and

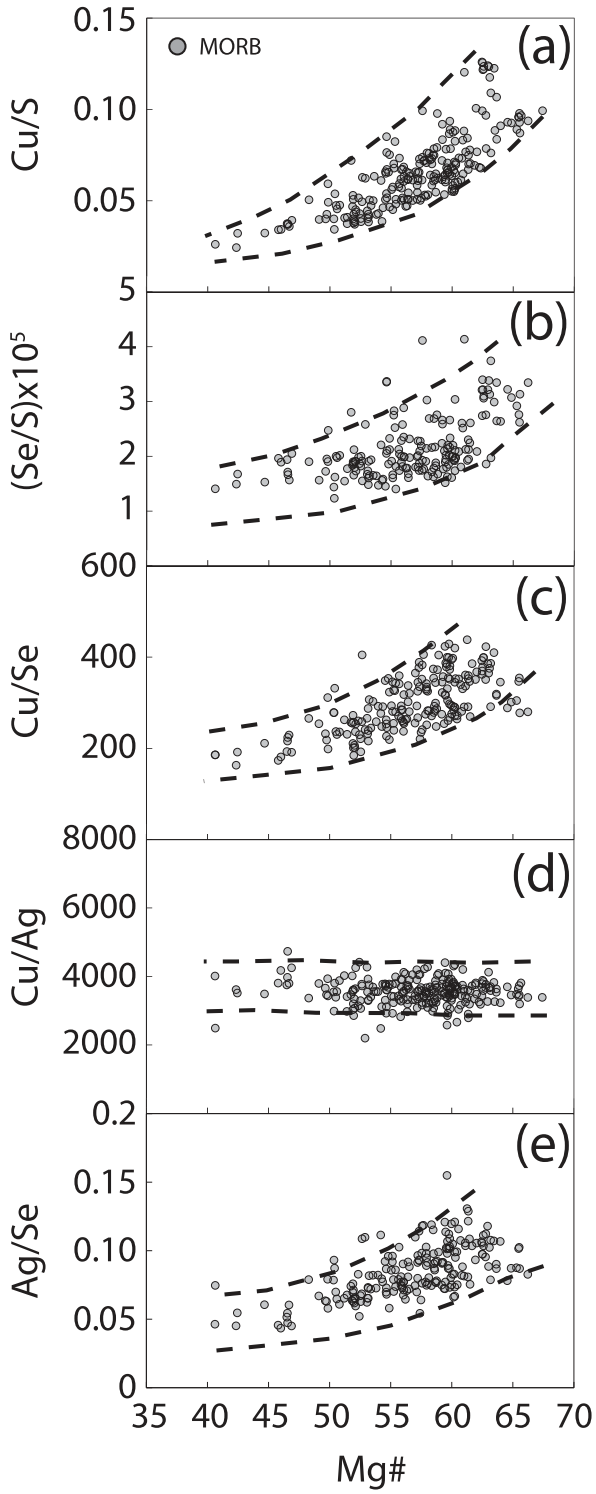

Fig. 3. Covariation diagrams showing variations in (a) Cu/S, (b) (Se/S) × 10^5, (c) Cu/Se, (d) Cu/Ag and (e) Ag/Se vs Mg-number for MORB.

clinopyroxene in the wet. Moreover, when plagioclase does appear in the crystallization of arc magmas, it is more anorthitic and consequently has lower SiO_2 than in dry magmas of comparable Ca/(Ca + Na). Fractional crystallization of the cpx and Ca-rich plagioclase assemblage in the wet magma series leads to a more rapid increase of SiO_2 than in MORB, in which SiO_2 increases only slowly with evolution by fractional crystallization.

Unlike MORB samples, which record a decrease in chalcophile element contents with continued fractional crystallization, resulting from saturation in a sulfide phase and its removal (Fig. 2), the contents of Cu, Se, Ag, and Au in the Manus Basin samples show an initial increase with decreasing Mg-number (Mg-number = 70–40; Fig. 5). This initially incompatible behaviour results in Cu, Ag, and Au enrichment in the melt to contents in excess of the MORB range. At an Mg-number of ~40 (corresponding to a SiO_2 content of ~60 wt %), magnetite saturates, which results in a decrease in FeO_{tot} V, TiO_2 and Re as each of these elements is compatible in magnetite (Fig. 4). The decrease in Re was earlier attributed to volatile loss during magma degassing (Sun *et al.*, 2003, 2004), but subsequently we have found Re is strongly compatible in magnetite (Mavrogenes *et al.*, 2008), explaining its correlation with FeO and TiO_2. The similarity in the partitioning behaviour of Re^{4+} and Ti^{4+} in basaltic systems was noted by Mallmann & O'Neill (2007). Following magnetite saturation, the plummet in Cu and Au, which was previously observed by Moss & Scott (2001) and Sun *et al.* (2004), is mirrored by Ag and importantly Se, indicating the appearance of a chalcophile-rich sulfide phase on the liquidus. There is also a marked decrease in the contents of P_2O_5 and Sr with continued fractionation at Mg-number < ~40, indicating the onset of apatite fractionation (Fig. 4).

The samples with the highest abundances of Cu, Ag, Se and Au have the same ratios of incompatible trace elements (e.g. La/Yb, Ta/Yb and Nb/U) as samples with SiO_2 >60 wt % (Fig. 6a–c). Thus, differences in the degrees of partial melting, variations in the composition of the mantle wedge, or assimilation of crustal material cannot explain the sudden change in the partitioning behaviour of many of the major and trace elements at ~60 wt % SiO_2 (Mg-number of ~40) in the Pual Ridge suite. Previous geochemical and isotopic studies present evidence for and against assimilation of crustal material associated with fractional crystallization during the genesis of magmas from the Manus Basin (e.g. Macpherson *et al.*, 2000; Shaw *et al.*, 2001; Sinton *et al.*, 2003; Park *et al.*, 2010). However, variations in Sr–Nd–Pb–O isotopic systematics and incompatible element systematics of the Eastern Manus Basin show no correlation with decreasing MgO (Macpherson *et al.*, 2000; Park *et al.*, 2010). Instead, Park *et al.* (2010) found decreases in $^{87}Sr/^{86}Sr$, Ba/La,

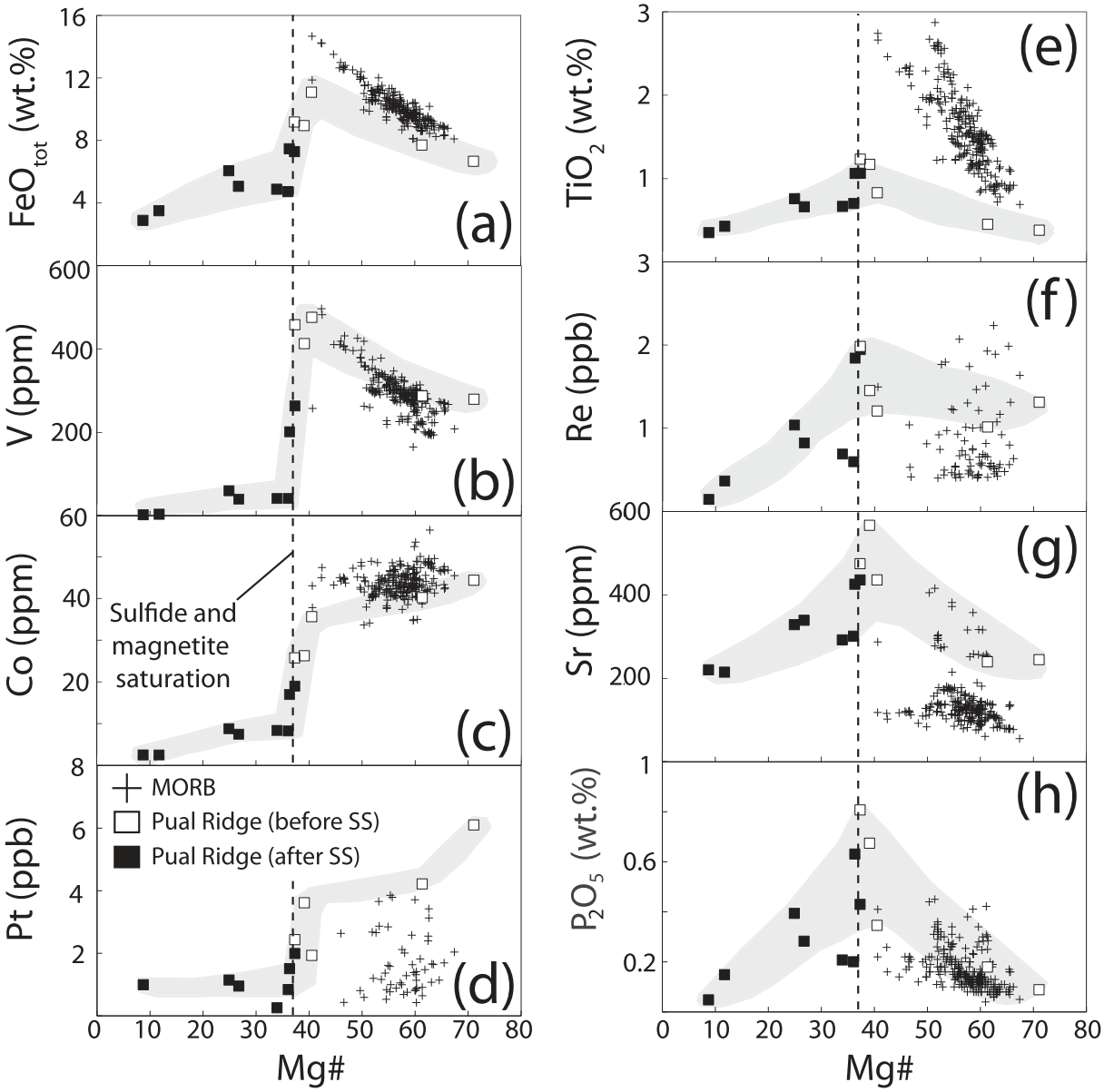

Fig. 4. Covariation of (a) FeO_{tot}, (b) V, (c) Co and (d) Pt, (e) TiO_2, (f) Re, (g) Sr and (h) P_2O_5 vs Mg-number in samples from the Pual Ridge compared with MORB. Mg and Fe (i.e. Mg-number) data for MORB from Melson *et al.* (2002). Shaded fields are used to emphasize the liquid line of descent of the Pual Ridge magmas. V, Co and Sr data for MORB from F. E. Jenner & H. S. C. O'Neill (unpublished data).

and Pb/Nd with increasing distance from New Ireland (i.e. from Susu Knoll to Pual Ridge; their figs 1 and 7), which indicate that the amount of the subduction component is the dominant control on the variations in isotopic systematics of magmas produced in the Eastern Manus Basin (Park *et al.*, 2010). The minor variations in $^{87}Sr/^{86}Sr$ of $0{\cdot}70370 \pm 0{\cdot}00009$ (2σ standard deviation) and the constant Nb/U (Fig. 6) within samples from the Pual Ridge indicate that crustal assimilation was inconsequential during magma differentiation.

VOLATILE EXSOLUTION OR SULFIDE SATURATION OF CHALCOPHILE ELEMENTS?

Moss & Scott (2001) and Sun *et al.* (2004) attributed the sudden drop in the contents of Au and Cu at magnetite saturation to pre-eruptive exsolution of a chalcophile-rich fluid or vapour phase. Our analyses reproduce the trends for Cu (Fig. 1) and Au, and show that Ag and importantly Se abundances also decrease abruptly at this

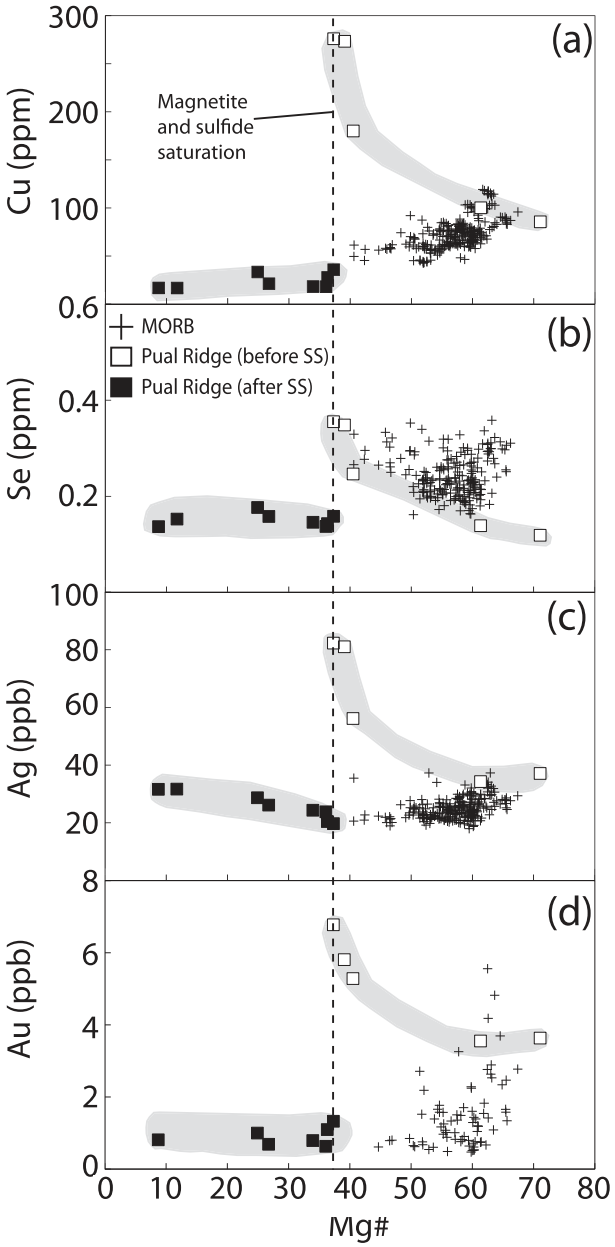

Fig. 5. Covariation of (a) Cu, (b) Se, (c) Ag, and (d) Au vs Mg-number. At an Mg-number of ~40 the contents of Cu, Ag and Au suddenly drop following magnetite fractionation. SS, sulfide saturation.

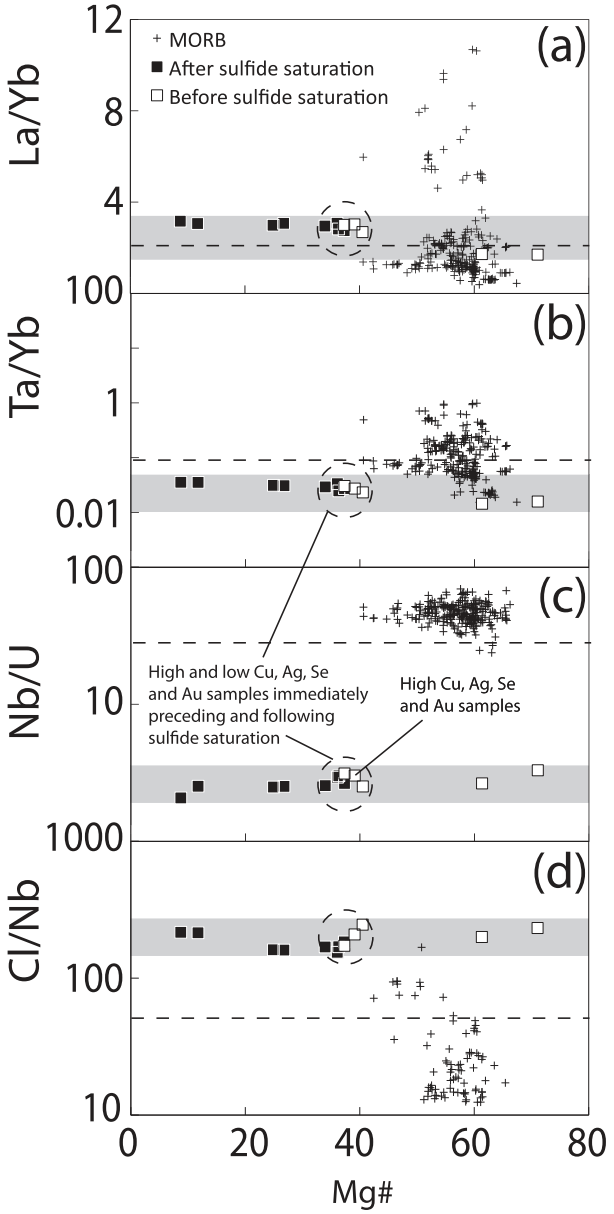

Fig. 6. Covariation of (a) La/Yb, (b) Ta/Yb, (c) Nb/U and (d) Cl/Nb vs Mg-number for the Pual Ridge samples compared with MORB (data for MORB from F. E. Jenner & H. S. C. O'Neill, unpublished data). Dashed circles show that the Pual Ridge samples immediately preceding (open squares) and following magnetite-triggered sulfide saturation (closed squares) have indistinguishable La/Yb, Ta/Yb, Nb/U and Cl/Nb, demonstrating that variations in the degree of partial melting, depletion of the mantle wedge, crustal assimilation and/or degassing cannot account for the differences in chalcophile element systematics of the Pual Ridge suite. Dashed lines show primitive mantle values from Palme & O'Neill (2003).

point (Fig. 5). The abundance of chlorine, an element with a propensity for partitioning into a fluid phase, increases with magmatic differentiation in the Pual Ridge suite, paralleling other highly incompatible elements ranging from moderately volatile (e.g. Cs, Sn, Pb, Bi) to refractory (e.g. W and La; Fig. 7); conservation of Cl in the magma during differentiation is well illustrated by the constant Cl/Nb of the Manus suite with decreasing Mg-number (Fig. 6). The behaviour of Cu, Au, Ag and Se is neither like that of S, which was lost during eruption from all Pual Ridge magmas regardless of their degree of evolution (Fig. 8), nor that of Cl (Figs 6 and 7). These

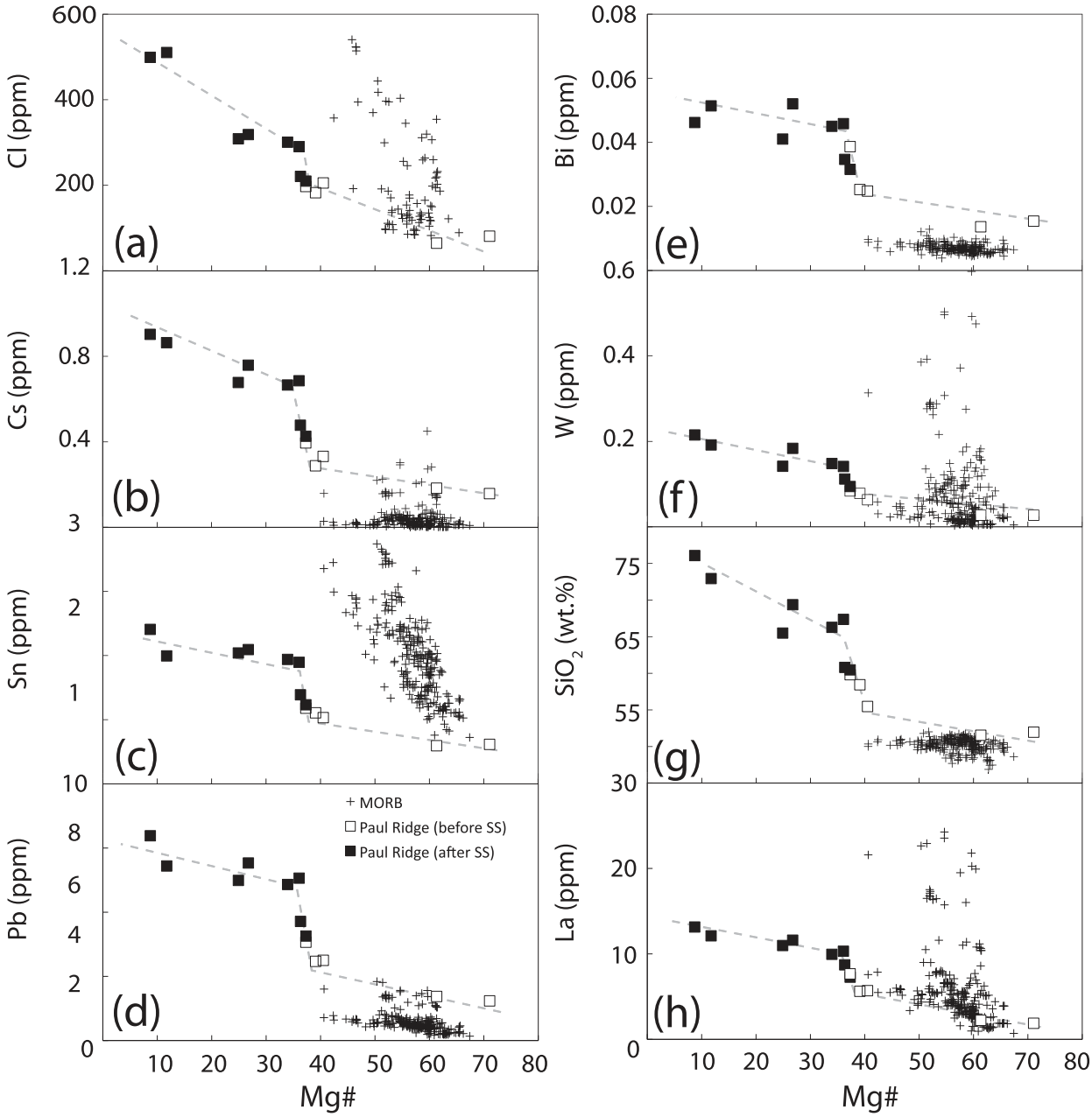

Fig. 7. Covariation of (a) Cl, (b) Cs, (c) Sn, (d) Pb, (e) Bi, (f) W, (g) SiO_2 and (h) La vs Mg-number, demonstrating that incompatible elements with a range in volatilities show no evidence of degassing during eruption. The break in slope at an Mg-number ~40 results from the rapid decrease in Mg-number associated with the sudden removal of Fe associated with magnetite fractionation. SS, sulfide saturation. Data for MORB from F. E. Jenner & H. S. C. O'Neill (unpublished data).

new data strengthen the argument that volatile exsolution did not produce the decrease in Cu, Au, Ag and Se contents.

Copper, Au, Ag and Se are all highly chalcophile, which suggests that the crystallization of magnetite-triggered saturation in a Cu-rich sulfide phase. This interpretation is supported by the change in chalcophile element ratios after the onset of magnetite fractionation (Fig. 9). Although it is possible that Cu could partition into magnetite, Se would not. Thus, the decrease in Se is as diagnostic of sulfide fractionation as V is of magnetite fractionation.

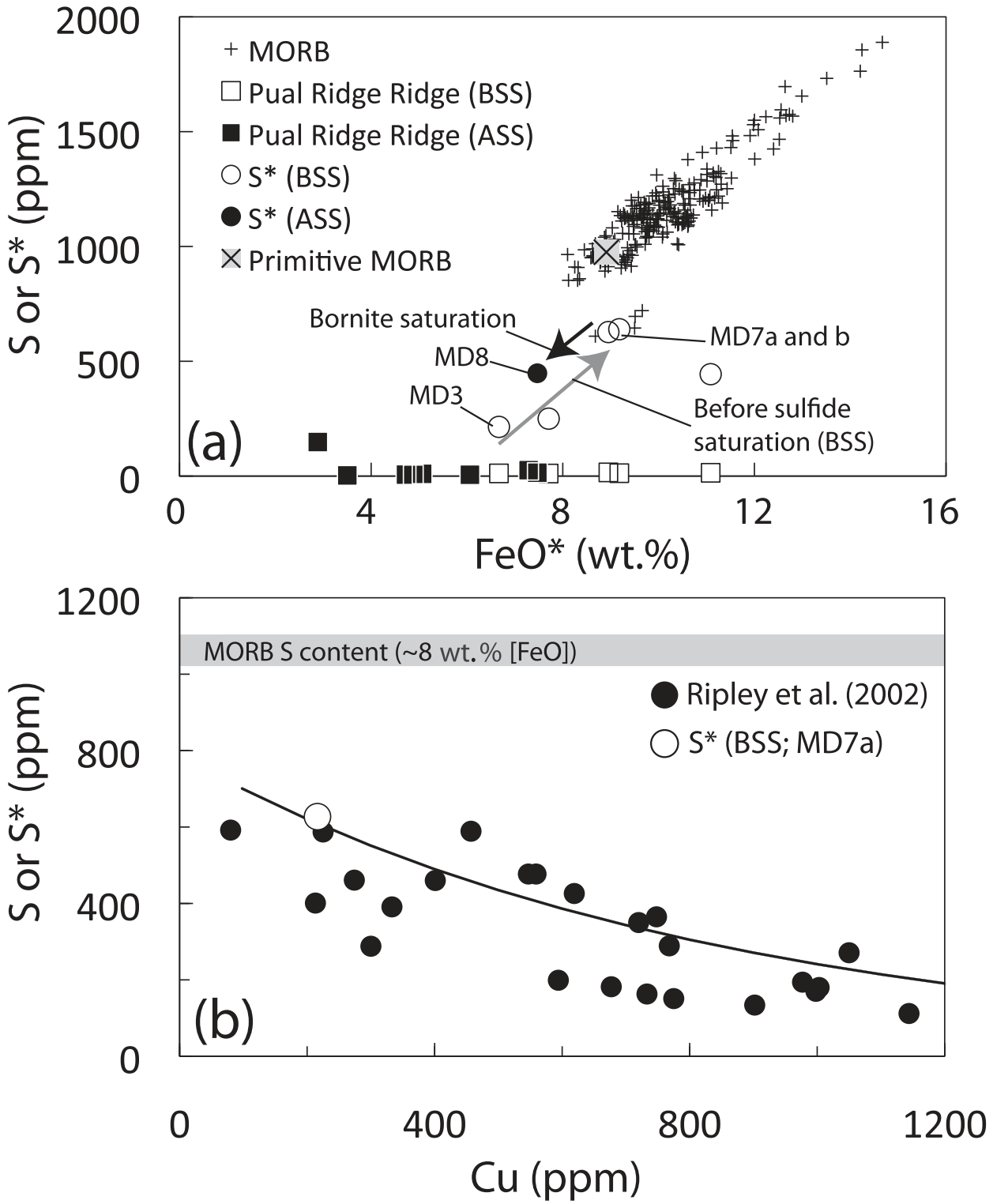

Fig. 8. Covariation of (a) S or S* vs FeO* (total Fe as FeO) for MORB compared with the samples from the Pual Ridge. The samples from the Pual Ridge (squares), both prior to and following magnetite-triggered sulfide saturation, have lost S by degassing. Circles show the estimated S contents (S*) for the Pual Ridge samples before sulfide saturation (BSS; open circles) and after sulfide saturation (ASS; closed circles). (b) S or S* vs Cu; sulfide saturation in Cu-rich, low-Ni magmas. The experimental data for the saturation of a basaltic melt with 4·7–8·5 wt % FeO in Cu–Fe–S–O sulfide melt at 1245°C is from Ripley *et al.* (2002) and are fitted to a semi-empirical expression accounting for the effect of FeO on sulfide saturation (continuous line).

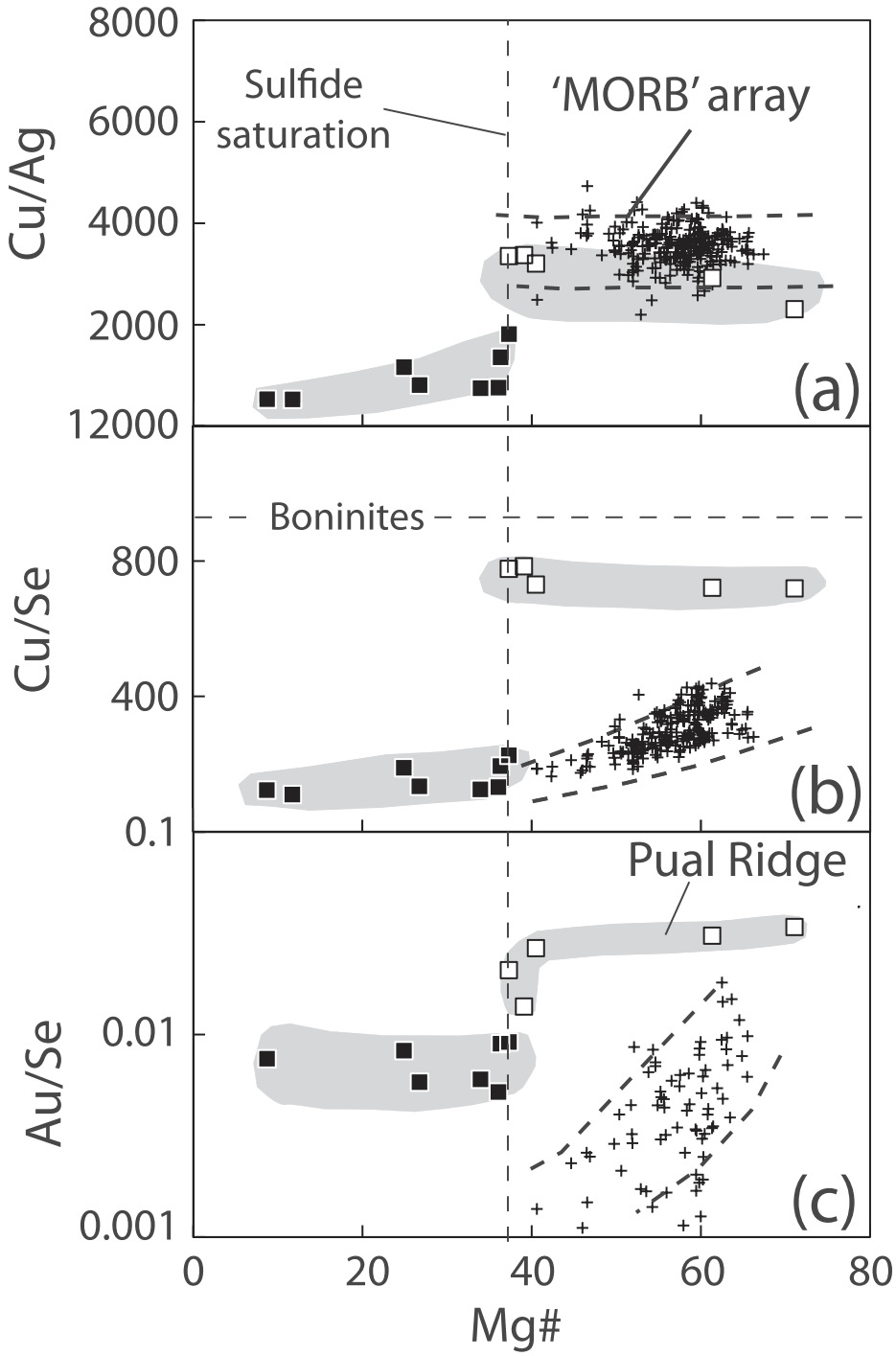

Fig. 9. Covariation of (a) Cu/Ag, (b) Cu/Se and (c) Au/Se vs Mg-number. (a) Prior to the onset of magnetite fractionation (Mg-number >40), the Pual Ridge samples have similar Cu/Ag to MORB. The onset of sulfide fractionation, prompted by magnetite fractionation, results in a decrease in the Cu/Ag, demonstrating that the sulfide fractionating from the Pual Ridge melts is different in composition from that fractionating from MORB, and is one in which Cu is more compatible than Ag. Prior to sulfide saturation, the Cu/Se of the Pual Ridge suite is intermediate between MORB and boninites (data for boninites from Hamlyn *et al.*, 1985), demonstrating that the residual sulfide in the mantle source region of the Pual Ridge magmas was more depleted than MORB. (b, c) The drop in Cu/Se and Au/Se at magnetite fractionation also points to a Cu-rich sulfide phase fractionating for the silicate melt.

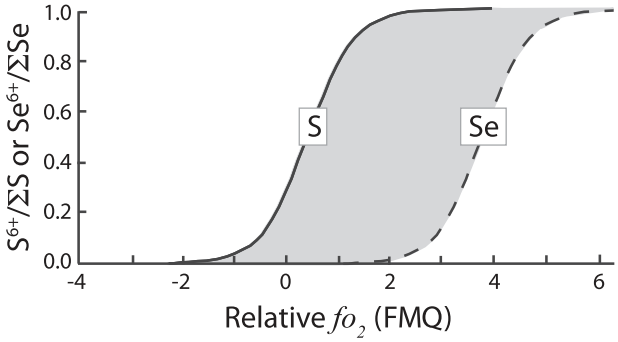

Fig. 10. Schematic diagram showing the higher predicted $S^{6+}/\sum S$ than $Se^{6+}/\sum Se$ (modified from Métrich & Clocchiatti, 1996) with increasing relative fO_2 with respect to FMQ. Grey field marks the field for samples from the Pual Ridge.

DECOUPLING OF SULFUR AND SELENIUM DURING ERUPTION AND DEGASSING

The hypothesis that Au, Cu, and Ag partition into a sulfide melt during evolution by fractional crystallization of arc and back-arc magmas has commonly been discounted because the measured contents of S appear to be far too low to achieve sulfide saturation (Sun *et al.*, 2004; Zajacz & Halter, 2009). However, S is typically degassed from volatile-containing melts with high fO_2 during eruption (Nilsson & Peach, 1993), so the content of S determined in the erupted volcanic rocks of a magma series is not a reliable indicator of the pre-eruptive (magma chamber) contents present during the evolution of a magma series. There is direct evidence for this late-stage loss of S in subduction-related settings from analyses of olivine-hosted melt inclusions, in which original S contents an order of magnitude greater than those in bulk erupted rocks are preserved (Métrich *et al.*, 1999; de Hoog *et al.*, 2001). All of the Pual Ridge samples from this study contain vesicles and are clearly degassed to the extent that virtually all S has been lost (Fig. 8). The scatter in S contents presented by Moss & Scott (2001) is also consistent with the propensity of S to exsolve during eruption. The key observation is that the contents of Se are similar to those in MORB (Fig. 5), indicating that the content of Se was not modified during degassing.

The main gaseous species of S in magmatic systems regardless of whether S is oxidized or reduced in the melt is SO_2 (Métrich *et al.*, 2009). In contrast, $SeO_2(g)$ is far less stable thermodynamically. Using available thermodynamic data, the equilibrium constant for the reaction

$$1 \cdot 042\,FeSe_{0.96}(s) + SO_2(g) = FeS(s) + SeO_2(g) + 0 \cdot 042\,Fe(s) \quad (1)$$

is −17·5 at 1000 K (data from Barin, 1989); unfortunately, data for stoichiometric FeSe are not available. Therefore, at these conditions the equilibrium ratio of SeO_2/SO_2 in the gas phase will be $\sim 10^{-8}$, implying that Se will not degas as SeO_2. Reduced magmas, in which sulfide is the dominant S species, retain S during eruption (quenching; i.e. MORB, Fig. 8a), yet oxidized, sulfate stable, quenched glasses contain little or no S. Thus, in the case of sulfur, the reduced species is retained whereas the oxidized species is lost. Se oxidizes to selenite or selenate at higher Eh, or fO_2 (e.g. Johnson & Bullen, 2004, and references therein) than the sulfide to sulfate transition, such that the topology may be as shown schematically in Fig. 10, where quenching in the shaded region loses oxidized sulfur but retains reduced Se. Experimental support for the much lower volatility of Se compared with S in silicate melts comes from the observation that the MPI-DING glass reference materials prepared from basaltic rocks in the laboratory at atmospheric pressure and high temperatures have lost almost all of their S, yet retained Se (Jochum *et al.*, 2006; Jenner *et al.*, 2009). Previous studies of the systematic behaviour of S and Se in geological samples have also shown that Se is far less mobile than S during hydrothermal alteration and metamorphism in low-temperature environments (Yamamoto, 1976; Howard, 1977; Lorand *et al.*, 2003; Barnes *et al.*, 2008).

ESTIMATING THE PRE-ERUPTIVE CONTENT OF SULFUR (S*) USING SELENIUM CONTENTS

Where degassing has lowered the S content of an erupted magma, Se is proposed as a proxy for estimating the pre-eruptive content of S. Prior to magnetite fractionation and sulfide saturation, the chalcophile element ratios of the Pual Ridge glasses (e.g. Cu/Ag and Cu/Se) are constant, as each element is incompatible in the silicate phases crystallizing from the evolving melt (Fig. 9). The build-up of Se, Cu, Ag and Au during fractionation of the Pual Ridge series, resulting from the high fO_2 of the silicate melt suppressing sulfide saturation [the oxidation state of MORB is lower than that of the samples from the Manus Basin (<FMQ), with $Fe^{3+}/\sum Fe = 0{\cdot}12$ (Bezos & Humler, 2005) compared with >0·2 (Sun *et al.*, 2004), respectively; Fig. 11], contrasts with the trends shown by the majority of MORB samples (Fig. 2), in which S contents, and hence also Se, Cu and Ag, are controlled by saturation with Fe–Ni-rich sulfide (Mathez, 1976). Thus, the S/Se of the Pual Ridge samples prior to sulfide saturation is assumed to remain constant. However, to use Se to estimate the S content of the parental the melts, an estimate of the original S/Se is required.

Variations in Ta/Yb can be used as a measure of the fertility of the mantle source region, as both elements are considered to show conservative behaviour during subduction

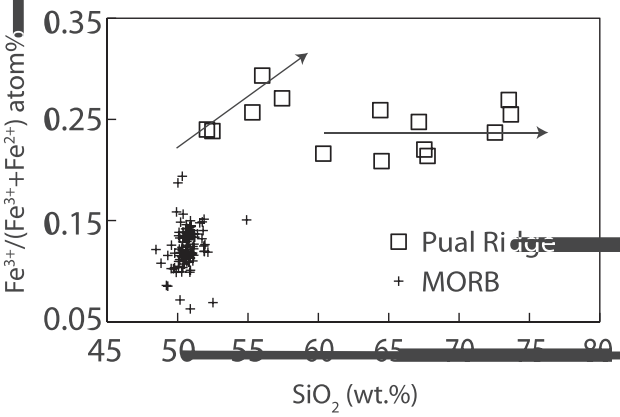

Fig. 11. Covariation of $Fe^{3+}/(Fe^{3+}+Fe^{2+})$ atom % vs wt % SiO_2 for the Pual Ridge samples (data from Sun *et al.*, 2004) compared with MORB data from Bezos & Humler (2005) shows an increase between ~50 and 60 wt % SiO_2 and sudden decrease at ~60 wt % SiO_2, supporting our interpretation that a change in fO_2 of the melt associated with magnetite fractionation triggers sulfide saturation.

(Pearce *et al.*, 2005). The lower Ta/Yb of the samples from the Pual Ridge compared with MORB (Fig. 6b) supports previous geochemical studies (e.g. Kamenetsky *et al.*, 2001; Sinton *et al.*, 2003), which argued that the mantle source region of the Pual Ridge magmas was more depleted by previous melt extraction than the source of MORB. It was pointed out by Hamlyn *et al.* (1985), in their study of boninites and other magnesian low-Ti magmas from subduction-related magmas, that prior depletion by melt extraction would probably cause the exhaustion (i.e. complete melting out) of the mantle sulfide component. Boninites are generally considered to have been generated by water-fluxed melting of extremely depleted mantle source regions (e.g. Crawford *et al.*, 1989).

The Se contents of the most primitive samples from the Pual Ridge are slightly lower than in MORB (Fig. 5), but higher than in the samples described by Hamlyn *et al.* (1985), except for a few samples from King Island. In contrast, the initial contents of Au, Ag and Cu are close to the upper range of MORB (Fig. 5). Hence, the Cu/Se, Ag/Se and Au/Se of the Pual Ridge samples prior to sulfide saturation are higher than in MORB (Fig. 9). These features are expected if the source of the Pual Ridge lavas was depleted in mantle sulfide by a prior melting event, but to a lesser extent than those studied by Hamlyn *et al.* (1985). Those workers found Cu/Se and Au/Se of ~900 and ~0·105, respectively, for boninites (average Cu/Se values of the Bonin Islands boninites are shown for comparison in Fig. 9).

Primitive MORBs from the Pacific and Atlantic oceans with >9 wt % MgO (Supplementary Data Table 1) have 975 ± 43 ppm S, and 0·291 ± 0·024 ppm Se (Fig. 7), such that S/Se = 3379 ± 291, somewhat higher than the estimated chondritic value of 2500 (Palme & O'Neill, 2003). This may be attributable to the original S/Se in the mantle being non-chondritic; as Palme & O'Neill (2003) pointed out, the S/Se in the Bulk Silicate Earth is only constrained rather poorly [see Rose-Weston *et al.* (2009) and references therein for a more recent appraisal of the available data]. Alternatively, the non-chondritic ratio may be due to fractionation of S/Se between silicate melt and residual sulfide melt in the genesis of MORB, because the in- [illegible] S/Se during the evolution of MORB (Fig. 8) shows that S/Se is lower in immiscible sulfide melt relative to silicate melt. Therefore, it is likely that the depleted source of the Pual Ridge samples would have had sulfide with lower S/Se than chondritic. For example, if MORB-source mantle had original S of 200 ppm with chondritic S/Se of 2500, and was depleted by extraction of MORB-like magma to form the source of the Pual Ridge magmas having only 100 ppm S, the S/Se of this residual sulfide would be 1800.

The pre-eruptive S content (S*) of the most primitive (highest Mg-number) glass (MD3) can then be estimated to be ~200 ppm. This is very much lower than MORB (open circles in Fig. 8). Thus, the parental melt would be undersaturated in sulfide, even if all the S in the magma was S^{2-}. Therefore, there are two reasons why the Pual Ridge magma can evolve without sulfide saturation: its high oxidation state and its low initial S. Assuming constant S/Se, the samples just prior to magnetite saturation (MD7a and MD7b) with 0·35 ppm Se will still have only ~600 ppm S, far below the level for sulfide saturation implied by the MORB array. However, the lack of sulfide fractionation has allowed the magmas to build up Cu contents that are several times those found in MORB.

THE MAGNETITE CRISIS

Magnetite fractionation triggers sulfide saturation

To constrain the effect of magnetite fractionation on the sulfide saturation point of relatively oxidized melts, we have investigated the phase relations of sample MD7b using the MELTS program (Ghiorso *et al.*, 2002). At the point at which a specified phase such as magnetite appears on the liquidus, a system of known composition at equilibrium has one degree of freedom thermodynamically, so by specifying pressure, we may calculate the liquidus temperature, the glass Fe^{3+}/Fe^{2+} (related to fO_2), and composition of the magnetite. At an assumed pressure of 0·2 GPa, with 1·5 wt % H_2O (Sun *et al.*, 2007), we find the liquidus of MD7b at 1095°C (see Thy & Lofgren, 1994), with $Fe^{3+}/\sum Fe$ in the melt of 0·29, giving an fO_2 relative to the fayalite–magnetite–quartz synthetic oxygen buffer (FMQ), log fO_2 = FMQ + 2·0. The $Fe^{3+}/\sum Fe$ data of Sun *et al.* (2004) are consistent with increasing Fe^{3+} up to the point of magnetite saturation and thereafter stabilization at a lower level (Fig. 11).

The magnetite on the liquidus has the composition $Fe^{2+}_{0\cdot93}Mg_{0\cdot24}Fe^{3+}_{1\cdot34}Al_{0\cdot24}Ti_{0\cdot21}O_4$; $Fe^{3+}/\sum Fe$ in this phase is 0·59, which is considerably higher than in the coexisting melt. An important point to emerge from MELTS modelling is that the oxidation state of the system (either $Fe^{3+}/\sum Fe$ or fO_2) required to trigger magnetite saturation is sensitive to the H_2O content of the melt: with the same major-element composition as MD7b, H_2O contents of 0·2%, 0·5% and 1·0% require that the melt has an $Fe^{3+}/\sum Fe$ of 0·45, 0·37 and 0·31, respectively.

At the calculated fO_2 of FMQ + 2, *c.* 90% of the S dissolved in the melt exists as SO_4^{2-} (Métrich & Clocchiatti, 1996, fig. 2). There is a homogeneous equilibrium in the melt between the redox couples Fe^{3+} and Fe^{2+} on one hand, and SO_4^{2-} and S^{2-} on the other (Métrich *et al.*, 2009):

$$SO_4^{2-} + 8\ Fe^{2+}O = S^{2-} + 8\ Fe^{3+}O_{1\cdot5} \qquad (2)$$

for which the equilibrium constant is

$$K = \left(\frac{Fe^{3+}/\sum Fe}{1 - Fe^{3+}/\sum Fe}\right)^8 \left(\frac{1-z}{z}\right) \qquad (3)$$

where z is the fraction of total S as SO_4^{2-}. Using $Fe^{3+}/\sum Fe = 0\cdot29$ and assuming $z = 0\cdot9$, $K = 8\cdot6 \times 10^{-5}$. The important point is that the stoichiometry of the reaction raises the Fe redox ratio (Fe^{3+}/Fe^{2+}) to the power of eight in the equilibrium constant. Consequently, a modest change in Fe redox ratio can have a great influence on sulfur speciation. A least-squares mass balance indicates that 2·6% magnetite of the composition found on the liquidus of MD7b must be subtracted from MD7b to give the next sample in the sequence (MD8), which causes $Fe^{3+}/\sum Fe$ to drop to 0·21, assuming closed-system conditions. Substituting this redox ratio into the equilibrium constant then gives $z = 0\cdot25$ for MD8; that is, the dissolved S in the melt switches from mostly SO_4^{2-} to mostly S^{2-}. We propose that this rapid switch in S redox ratio, triggered by the calculated amount of magnetite fractionation, causes saturation in a sulfide phase, and hence the sudden drop in Cu, Au, Ag and Se, in glasses richer than 60 wt % SiO_2 and with an Mg-number of <40 in the magma series (Fig. 5). Magnetite fractionation triggering sulfide saturation may be a common occurrence in the evolution of magmas, and has previously been suggested as the mechanism producing the Platinova reef of the Skaergaard intrusion (Andersen, 2006), and the PGE mineralization associated with magnetite in the Stella layered intrusion of South Africa (Maier *et al.*, 2003).

Magnetite fractionation triggers apatite saturation

The decrease in P_2O_5 (Fig. 5) at an Mg-number of ~40 argues that magnetite fractionation also triggers saturation in apatite as well as precipitating sulfide. The dominant controls on apatite saturation are the activities of P_2O_5, SiO_2, Al_2O_3 and CaO, and temperature (e.g. Watson, 1979; Harrison & Watson, 1984; Sha, 2000; Tollari *et al.*, 2006), but none of these factors change much with the precipitation of 2·6% magnetite, which mainly affects Fe contents and oxidation state.

Toplis *et al.* (1994*a*) showed that increasing P in the melt increases the solubility of magnetite, which they attributed to stable $Fe^{3+}(PO_4)^{3-}$ complexes in the melt. However, this explanation seems inconsistent with the effect that adding P has on lowering Fe^{3+}/Fe^{2+} in silicate melts (Mysen, 1992; Toplis *et al.*, 1994*b*; Jayasuriya *et al.*, 2004). Whatever the mechanism, the corollary should be that the decrease in Fe^{3+} following magnetite fractionation should indeed lower the solubility of P and favour the promotion of apatite to a liquidus phase. Tollari *et al.* (2006) tested this hypothesis explicitly by varying total Fe content and fO_2 and concluded that 'neither iron content of the liquid nor oxidation state play a significant role on phosphate saturation'. Nevertheless, their experimental results clearly showed a positive correlation between P_2O_5 and Fe_2O_3 (calculated from total Fe and fO_2) except at very high P_2O_5 where molar P/Fe > 1 (e.g. Tollari *et al.*, 2006, fig. 5).

Parat & Holtz (2004) found a barely resolvable increase in apatite solubility in SO_4^{2-}-containing melts compared with S-free melts at similar conditions. However, these results are for melts with low CaO contents (<0·7 wt %) in which formation of $Ca–SO_4^{2-}$ complexes might affect the activity of CaO. Hence, this scenario is unlikely in the much higher Ca, lower S compositions of the Pual Ridge magmas. The reason for the coincidence of magnetite and apatite saturation therefore remains enigmatic, although we note that there seem to be frequent occurrences of apatite inclusions in magnetite in igneous rocks (e.g. Frietsch & Perdahl, 1995; Gelcich *et al.*, 2005).

THE NATURE OF THE SULFIDE PHASE AT THE MAGNETITE CRISIS

Another reason why the role of sulfide precipitation may have been overlooked in the Pual Ridge suite is that many of the other chalcophile or potentially chalcophile elements analysed for this study do not show the same abrupt decrease as Cu, Au, Ag and Se at Mg-number ≈ 40. Rather, these other elements (e.g. Co, Ni, As, Sn, Sb, Re, Pt, Pb and Bi) either do not decrease at all (e.g. As) or show a moderate decrease that may be attributed to the fractionation of magnetite, chromite, olivine and clinopyroxene (e.g. Co and Ni). We propose that this apparent inconsistency may be explained by the nature of the sulfide phase, which is expected to be very different from the

sulfide in equilibrium with MORB. Examination of sulfide globules in MORB glasses shows that this phase is an Fe–Ni-rich sulfide melt with approximately the stoichiometry of monosulfide solid solution (e.g. Mathez, 1976). MORBs evolve saturated with sulfide liquid, the composition of which has been inferred from the sulfide globules in MORB glasses (Mathez, 1976; Czamanske & Moore, 1977; Francis, 1990). These globules are composed of finely intergrown Fe–Ni–Cu-sulfides that crystallize on quenching of the original sulfide melt. The parent sulfide liquid probably also contained a few weight per cent of oxygen (Fonseca *et al.*, 2008), which quenches to magnetite (Czamanske & Moore, 1977). Czamanske & Moore (1977) showed that the composition of the globules changes with increasing evolution of MORB, decreasing from Ni-rich [Ni/(Ni + Fe + Cu) ≈ 0·25] in the most primitive MORB glasses, to Ni-poor [Ni/(Ni + Fe + Cu) ≈ 0·05] in the more evolved (see Czamanske & Moore, 1977, fig. 4). The average composition of the MORB sulfide globules analysed by Francis (1990) is Fe 46 wt %, Ni 7 wt %, Cu 10 wt % and S 36 wt %, from glasses covering a large range of MgO, from 10·0 wt % (primitive MORB), to 5·4 wt %. The Pual Ridge magmas at the magnetite crisis have higher Cu and considerably lower Ni contents than MORB and consequently will fractionate sulfide that is more Cu-rich and Ni-poor. Furthermore, the S content of the Pual Ridge magmas at the magnetite crisis estimated above from S/Se systematics at ~600 ppm is only half that of sulfide-saturated MORB with similar FeO_{tot} (Fig. 8a).

The Cu/Ag of MORB remains constant with decreasing Mg-number (Fig. 3), which demonstrates that the partition coefficient of Ag between silicate melt and the MORB sulfide phase is similar to that of Cu. In contrast, the onset of sulfide saturation in the Pual Ridge suite causes a marked decrease in the Cu/Ag of the residual melt, and Cu/Ag continues to decrease with further evolution (Fig. 9). This change in Cu/Ag implies that Cu is more compatible in the sulfide fractionating from the Pual Ridge suite than Ag. Analysis of chalcophile element abundances in a range of sulfides has shown that the Cu/Ag of chalcopyrite is considerably higher than that in pyrrhotite (Barnes *et al.*, 2008) and that the content of Ag is considerable higher in Cu-rich sulfides. In the Cu–Fe–S system, intermediate solid solution (ISS, the high-temperature equivalent of chalcopyrite) is not stable above 960°C, whereas bornite (ideal formula Cu_5FeS_4) is stable at the calculated liquidus temperature of MD7b of ~1095°C; (Kullerud *et al.*, 1969; Ebel & Naldrett, 1997).

Assuming that the drop in Cu content, Δ[Cu], between samples MD7b and MD8 of 250 ppm resulted from sulfide fractionation, we can constrain approximately the composition of the sulfide phase by using the drop in S as calculated from the drop in Se and some estimate of the S/Se systematics:

$$\Delta[S^*] = \Delta[Se] \times (S/Se)^{sulfide} \quad (4)$$

where Δ[Se] is the change in Se content resulting from sulfide fractionation between samples MD7b and MD8 (in this case 0·21 ppm). Only limited measurements ($n = 4$) of the content of Se in bornite are available in the literature and show a large range in S/Se from 646 to 1280 (Core *et al.*, 2006) and an average of 931 ±268. Thus, the average Δ[S*] calculated using the available bornite analyses is 192 ± 57 ppm, S* in MD8 is ~450 ppm and the Cu/S in the sulfide phase is estimated as 1·38 ± 0·37, within uncertainty of that expected from the stoichiometry of bornite. Segregation of a crystalline Cu sulfide as opposed to Fe–Ni-rich sulfide matte or monosulfide solid solution explains the depletion in Ag and Au, elements that occur in sulfides with a similar valence to Cu (1+), favouring their partitioning into bornite, unlike other potentially strongly chalcophile elements such as Ni, Re, and Pt with higher valence states, which do not show the abrupt decrease (Fig. 4). S* in the melt prior to sulfide saturation is estimated as only ~640 ppm; below the sulfur-saturated MORB array (Fig. 8). However, this estimate is within the range of Cu and S contents in experimental Cu-rich, Ni-poor basaltic melts with 4·7–8·5 wt % FeO, saturated in Cu–Fe–S–O sulfide melt at 1245°C [Fig. 8b; data from Ripley *et al.* (2002)]. Scatter in the experimental data from Ripley *et al.* (2002) in this two-variable plot is caused by variations in FeO. To adjust for this, we have fitted the data to a semi-empirical expression accounting for the effect of FeO on sulfide saturation [see equation (27) of O'Neill & Mavrogenes 2002]):

$$\ln[S]_{SulfSat} = 6 \cdot 98 + 0 \cdot 22[FeO] - \ln[FeO] - 0 \cdot 0096[Cu]/[FeO] \quad (5)$$

where [FeO] is total Fe as FeO in the silicate melt (in wt %), and [S] and [Cu] are the contents in the silicate melt (in ppm). For the Pual Ridge magma at the magnetite crisis, [Cu] is 275 ppm and [FeO] is 8 ppm, hence $[S]_{SulfSat}$ is calculated to be 560 ppm, in agreement with S* estimated from S/Se systematics of ~640 ppm at the magnetite crisis. The great thermodynamic stability of Cu-rich sulfides causes them to saturate at lower levels of dissolved S^{2-} in the silicate melt (e.g. Evans *et al.*, 2008*a*), compared with sulfide saturation in anhydrous melts such as MORB. The presence of small magmatic chalcopyrite and bornite inclusions in magnetite (e.g. Borrok *et al.*, 1999) lends support to the hypothesis that magnetite fractionation may precipitate Cu-rich sulfides. The hypothesis that this phase may be crystalline bornite, given sufficiently low magmatic temperatures, as in the H_2O-containing Pual Ridge magma series, is amenable to experimental

testing, as is the idea that such a phase would sequester Ag and Au but not other potentially chalcophile elements.

ENRICHMENT OF ORE METALS IN OXIDIZED MELTS FROM INITIAL 'MORB'-LIKE CONTENTS

There is a well-known association between Au–Cu-rich sulfide deposits and convergent margins (e.g. Hedenquist & Lowenstern, 1994; Sillitoe, 2010, and references therein). However, economically mineable deposits are not produced in all subduction-related settings. In this study we have shown that the most primitive samples from the arc-like Pual Ridge, Eastern Manus Basin, are depleted in FeO_{tot} (Fig. 4), Se (Fig. 5), and probably S compared with MORB-related samples. The contents of Au, Cu, and Ag (Fig. 5) are within the range of MORB, indicating that their contents are not greatly enriched in the mantle wedge by fluid ingress from the subducting slab. Low abundances of Se and Cu in arc-related low-Ti lavas and boninites have previously been identified by Hamlyn *et al.* (1985). They used the systematic relationships between Mg-number, Se, and Ti to argue that the mantle wedge component becomes increasingly S-undersaturated and depleted in chalcophile elements with continued melt extraction, and found no evidence for addition of chalcophile elements during mantle metasomatism. The initial budget of S and chalcophile elements in magmas generated in subduction-related settings is probably controlled by the presence of sulfide phases in the mantle wedge, sulfur solubility during partial melting (e.g. the content of FeO in the melt), and ultimately the fertility of the wedge component as opposed to enrichment from the subducting slab. The lower Ta/Yb (Fig. 6b) and initial Se and FeO_{tot} (Figs 4 and 5) of the Pual Ridge suite compared with MORB is in agreement with the interpretations of Hamlyn *et al.* (1985) that the mantle wedge becomes progressively depleted in chalcophile elements with continued melt extraction. The high Cu/Se and Ag/Se of the Pual Ridge suite compared with MORB (Fig. 9) demonstrates that Cu and Ag are more compatible in mantle sulfides than Se, and that the mantle source region will evolve to higher Cu/Se and Ag/Se with progressive melt removal.

Differentiation of S-undersaturated, moderately to highly oxidized arc magmas prior to magnetite-triggered sulfide saturation, results in the enrichment of Cu (~280 ppm), Ag (~90 ppb) and Au (~7 ppb) to contents considerably higher than MORB (Fig. 5). The low S* and high fO_2 of the Manus Basin magmas suppresses the early segregation of magmatic sulfide, otherwise ubiquitous in MORB. Experimental studies demonstrate that crystallization of pyrrhotite from low-fO_2 magmas such as MORB depletes the magma in Cu (Jugo *et al.*, 1999), preventing the dramatic increase in Cu from 50 to 60 wt % SiO_2 seen in the Pual Ridge suite (Fig. 5). We emphasize that the oxidized nature of arc-related magmas is the key feature leading to their enrichment in chalcophile elements relative to other tectonic environments. Arc-type sulfide-undersaturated, oxidized melts experience a prolonged interval of 'sulfide-free' fractionation; the sulfide eventually formed is rich in Au, Cu, and Ag. High H_2O contents of arc-related magmas also help to bring magnetite onto the liquidus at a relatively early stage of magma evolution. It is unnecessary to invoke an enriched mantle source resulting from addition of S and chalcophile elements via a subduction-derived component (e.g. Stolper & Newman, 1994; de Hoog *et al.*, 2001; Mungall, 2002).

Sulfide-rich enclaves within the earliest unaltered intrusive phases of the Bingham (Utah, USA) giant porphyry copper deposit, the Last Chance Stock, consist of clinopyroxene, biotite, magnetite, ilmenite and plagioclase with accessory sulfides including 2% bornite and 0·3% chalcopyrite, and have been interpreted to have formed by low-pressure crystallization of the host magma (Core *et al.*, 2006). Microprobe analyses of these sulfides show enrichments in Au, Ag, and Se. It has been suggested that the parental magma of the Last Chance Stock was generated by partial melting of mafic lower crustal material containing Cu-rich sulfide cumulates, resulting in the production of Cu-rich melts (Vogel *et al.*, 2001; Core *et al.*, 2006). Partial melting of Cu–Ag–Au-rich bornite cumulate layers within magma chambers integral to subduction-related systems such as those of the Manus Basin is a possible process for generating Cu-rich intermediate magmas such as those of the Last Chance Stock. Alternatively, fluids transgressing or leaching Cu–Au–Ag intracrustal cumulate sulfide horizons will dissolve high contents of these ore-forming metals; we note that arc and back-arc basin hydrothermal sulfide deposits have higher Au contents than those that precipitate on the sea floor in non-convergent margin settings (Herzig *et al.*, 1993).

CONCLUSIONS

In summary, the low contents of chalcophile elements in the most primitive Pual Ridge samples are comparable with those in MORB, indicating that these elements are not enriched in the mantle wedge. The suppression of sulfide as a liquidus phase in arc-related melts with high fO_2 allows Cu, Ag, Au, S, and Se to become enriched during magmatic evolution by fractional crystallization. Eventually, the appearance of magnetite on the liquidus lowers the FeO_{tot}, Fe_2O_3, and SO_4/S^{2-} of the melt, and triggers sulfide saturation. The saturation of the melt in sulfide is concomitant with apatite saturation. Because this saturation occurs in relatively evolved magmas with low Ni but high Cu compared with MORB, the sulfide phase is bornite rather than the Ni–Fe-rich sulfide

(monosulfide solid solution) typical of MORB (e.g. Mathez, 1976). This phenomenon is not observed in melts with low fO_2 (i.e. MORB) as the immiscible sulfide on the liquidus of even the most primitive magmas prevents the build-up of Cu, Ag and Au. In contrast, the bornite fractionation inferred to accompany the appearance of magnetite on the liquidus is the critical first step in the enrichment of Cu, Ag and Au in subduction-related settings. This first step should result in the formation of oxide–sulfide horizons in sub-arc plutonic sequences.

ACKNOWLEDGEMENTS

We thank Charlotte Allen and Rob Rapp for technical support and for ensuring that the LA-ICP-MS system and electron microprobe are well cared for. Jeremy Wykes and Jung Park are thanked for discussions pertaining to this contribution. Matthew Leybourne, Jeff Mauk and an anonymous reviewer are thanked for their thoughtful reviews. We would also like to thank the Department of Mineral Sciences, US National Museum of Natural History, Washington, DC for providing a beautiful collection of MORB volcanic glasses for this project.

FUNDING

The work was supported by a grant from the Australian Research Council to J.A.M. and R.J.A.

SUPPLEMENTARY DATA

Supplementary data for this paper are available at *Journal of Petrology* online.

REFERENCES

Andersen, J. C. Ø. (2006). Post magmatic sulphur loss in the Skaergaard intrusion: implications for the formation of the Platinova reef. *Lithos* **92**, 198–221.

Arculus, R. J. (2004). Evolution of arc magmas and their volatiles. In: Sparks, R. S. J. & Hawkesworth, C. J. (eds) *The State of the Planet: Frontiers and Challenges in Geophysics. Geophysical Monograph, American Geophysical Union* **150**, 95–108.

Barin, I. (1989). *Thermochemical Data of Pure Substances, Part I and II*. Weinheim, VCH, 1739 p.

Barnes, S.-J., Prichard, H. M., Cox, R. A., Fisher, P. C. & Godel, B. (2008). The location of the chalcophile elements and siderophile elements in platinum-groups element deposits (a textural, microbeam and whole rock geochemical study): Implications for the formation of the deposits. *Chemical Geology* **248**, 295–317.

Barnes, S.-J., Savard, D., Bédard, L. P. & Maier, W. D. (2009). Selenium and sulfur concentrations in the Bushveld Complex of South Africa and implications for formation of the platinum-group element deposits. *Mineralium Deposita* **44**, 647–663.

Bezos, A. & Humler, E. (2005). The Fe^{3+}/Sigma Fe ratios of MORB glasses and their implications for mantle melting. *Geochimica et Cosmochimica Acta* **69**, 711–725.

Binns, R. A. & Scott, S. D. (1993). Actively forming polymetallic sulfide deposits associated with felsic volcanic rocks in the Eastern Manus back-arc Basin, Papua New Guinea. *Economic Geology* **88**, 2226–2236.

Borrok, D., Kesler, S. E. & Vogel, T. A. (1999). Sulfide mineral in intrusive and volcanic rocks of the Bingham–Park City Belt, Utah. *Economic Geology* **94**, 1213–1230.

Core, D. P., Kesler, S. E. & Essene, E. J. (2006). Unusually Cu-rich magmas associated with giant porphyry copper deposits: Evidence from Bingham, Utah. *Geology* **34**, 41–44.

Crawford, A. J., Falloon, T. J. & Green, D. H. (1989). Classification, petrogenesis and tectonic setting of boninites. In: Crawford, A. J. (ed.) *Boninites and Related Rocks*. London: Unwin Hyman Ltd., pp. 1–49.

Czamanske, G. K. & Moore, J. G. (1977). Composition and phase chemistry of sulfide globules in basalts from the Mid-Atlantic-Ridge rift valley near 37°N lat. *Geological Society of America Bulletin* **88**, 587–599.

de Hoog, J. C. M., Mason, P. R. D. & van Bergen, M. J. (2001). Sulfur and chalcophile elements in subduction zones: constraints from a laser ablation ICP-MS study of melt inclusions from Galunggung Volcano, Indonesia. *Geochimica et Cosmochimica Acta* **65**, 3147–3164.

Doe, B. (1995). Zinc, copper, and lead geochemistry of oceanic igneous rocks—ridges, islands, and arcs. *International Geology Review* **37**, 379–420.

Doe, B. R. (1994). Zinc, copper, and lead in mid-ocean ridge basalts and the source rock control on Zn/Pb in ocean-ridge hydrothermal deposits. *Geochimica et Cosmochimica Acta* **58**, 2215–2223.

Ebel, D. S. & Naldrett, A. J. (1997). Crystallisation of sulfide liquids and the interpretation of ore composition. *Canadian Journal of Earth Sciences* **34**, 352–365.

Eggins, S. (2003). Laser ablation ICP-MS analysis of geological materials prepared as lithium borate glasses. *Geostandards Newsletter* **27**, 147–162.

Eggins, S. M. & Shelley, J. M. G. (2002). Compositional heterogeneity in NIST SRM 610–617 glasses. *Geostandards and Geoanalytical Research* **26**, 269–286.

Evans, K. A., O'Neill, H. S. C. & Mavrogenes, J. A. (2008*a*). Sulphur solubility and sulphide immiscibility in silicate melts as a function of the concentration of manganese, nickel, tungsten and copper at 1 atm and 1400°C. *Chemical Geology* **255**, 236–249.

Evans, T. M., O'Neill, H. S. C. & Tuff, J. (2008*b*). The influence of melt composition on the partitioning of REEs, Y, Sc, Zr and Al between forsterite and melt in the system CMAS. *Geochimica et Cosmochimica Acta* **72**, 5708–5721.

Fonseca, R. O. C., Campbell, I. H., O'Neill, H. S. C. & Fitz Gerald, J. D. (2008). Oxygen solubility and speciation in sulphide-rich mattes. *Geochimica et Cosmochimica Acta* **72**, 2619–2635.

Francis, R. D. (1990). Sulfide globules in mid-ocean ridge basalts (MORB), and the effect of oxygen abundance in Fe–S–O liquids on the ability of those liquids to partition metals from MORB and komatiite magmas. *Chemical Geology* **85**, 199–213.

Frietsch, R. & Perdahl, J.-A. (1995). Rare earth elements in apatite and magnetite in Kiruna-type iron ores and some other iron ore types. *Ore Geology Reviews* **9**, 489–510.

Gaboardi, M. & Humayun, M. (2009). Element fractionation during LA-ICP-MS analyses of silicate glasses: implications for matrix-independent standardization. *Journal of Analytical Atomic Spectrometry* **24**, 1188–1197.

Gelcich, S., Davis, D. W. & Spooner, E. T. C. (2005). Testing the apatite–magnetite geochronometer: U–Pb and $^{40}Ar/^{39}Ar$ geochronology of plutonic rocks, massive magnetite–apatite tabular bodies, and IOCG mineralization in Northern Chile. *Geochimica et Cosmochimica Acta* **69**, 3376–3384.

Ghiorso, M. S., Hirschmann, M. M., Reiners, P. W. & Kress, V. C., III (2002). The pMELTS; a revision of MELTS for improved calculation of phase relations and major element partitioning related to partial melting of the mantle to 3 GPa. *Geochemistry, Geophysics, Geosystems* **3**, doi:10.1029/2001GC000217.

Hamlyn, P. R., Keays, R. R., Cameron, W. E., Crawford, A. J. & Waldron, H. M. (1985). Precious metals in low-Ti lavas: Implications for metallogenesis and sulfur saturation in primary magmas. *Geochimica et Cosmochimica Acta* **49**, 1797–1811.

Harrison, T. M. & Watson, E. B. (1984). The behavior of apatite during crustal anatexis: Equilibrium and kinetic considerations. *Geochimica et Cosmochimica Acta* **48**, 1467–1477.

Hedenquist, J. W. & Lowenstern, J. B. (1994). The role of magmas in the formation of hydrothermal ore deposits. *Nature* **370**, 519–527.

Hertogen, J., Janssens, M. J. & Palme, H. (1980). Trace-elements in ocean ridge basalt glasses—implications for fractionations during mantle evolution and petrogenesis. *Geochimica et Cosmochimica Acta* **44**, 2125–2143.

Herzig, P. M., Hannington, M. D., Fourquet, Y., von Stackelberg, U. & Petersen, S. (1993). Gold-rich polymetallic sulfides from the Lau back arc and implications for the geochemistry of gold in sea-floor hydrothermal systems of the Southwest Pacific. *Economic Geology* **88**, 2182–2209.

Howard, J. H. (1977). Geochemistry of selenium: formation of ferroselite and selenium behavior in the vicinity of oxidising sulfide and uranium deposits. *Geochimica et Cosmochimica Acta* **41**, 1665–1678.

Hu, Z., Liu, Y., Li, M., Gao, S. & Zhao, L. (2009). Results for rarely determined elements in MPI-DING, USGS and NIST glasses using laser ablation ICP-MS. *Geostandards and Geoanalytical Research* **33**, 319–335.

Humayun, M., Simon, S. B. & Grossman, L. (2007). Tungsten and hafnium distribution in calcium–aluminum inclusions (CAIs) from Allende and Efremovka. *Geochimica et Cosmochimica Acta* **71**, 4609–4627.

Jayasuriya, K. D., O'Neill, H. S. C., Berry, A. J. & Campbell, S. J. (2004). A Mössbauer study of the oxidation state of Fe in silicate melts. *American Mineralogist* **89**, 1597–1609.

Jenner, F. E., Holden, P., Mavrogenes, J. A., O'Neill, H. S. C. & Allen, C. (2009). Determination of selenium concentrations in NIST SRM 610, 612, 614 and geological glass reference materials using the electron probe, LA-ICP-MS and SHRIMP II. *Geostandards and Geoanalytical Research* **33**, 309–317.

Jochum, K. P. & Stoll, B. I. (2008). Reference materials for elemental and isotopic analyses by LA-(MC)-ICP-MS: successes and outstanding needs. In: Sylvester, P. (ed.) *Laser Ablation ICP-MS in the Earth Sciences: Current practices and outstanding issues*. Mineralogical Association of Canada. Short Course Volume 40, pp. 147–168.

Jochum, K. P., Stoll, B., Herwig, K., Willbold, M. & Hoffman, A. W. (2006). MPI-DING reference glasses for *in situ* microanalysis: New reference values for element concentrations and isotope ratios. *Geochemistry, Geophysics, Geosystems* **7**, doi:10.1029/2005GC001060.

Johnson, T. M. & Bullen, T. D. (2004). Mass-dependent fractionation of selenium and chromium isotopes in low-temperature environments. In: Johnson, C. M., Beard, B. L. & Albarède, F. (eds) *Geochemistry of Non-traditional Stable Isotopes. Mineralogical Society of America and Geochemical Society, Reviews in Mineralogy and Geochemistry* **55**, 289–317.

Jugo, P. J., Candela, P. A. & Piccoli, P. M. (1999). Magmatic sulfides and Au:Cu ratios in porphyry deposits: An experimental study of copper and gold partitioning at 850°C, 100 MPa in a haplogranitic melt–pyrrhotite intermediate solid solution–gold metal assemblage, at gas saturation. *Lithos* **46**, 573–589.

Kamenetsky, V. S., Binns, R. A., Gemmell, J. B., Crawford, A. J., Mernagh, T. P., Maas, R. & Steele, D. (2001). Parental basaltic melts and fuids in eastern Manus backarc Basin: implications for hydrothermal mineralisation. *Earth and Planetary Science Letters* **184**, 685–702.

Kullerud, G., Yund, R. A. & Moh, G. H. (1969). Phase relations in the Cu–Fe–S, Cu–Ni–S and Fe–Ni–S systems. In: Wilson, H. D. B. (ed.) *Magmatic Ore Deposits: a Symposium*. Lancaster, PA: Economic Geology Publishing Co., pp. 323–343.

Longerich, H. P., Jackson, S. E. & Günther, D. (1996). Elemental fractionation in laser ablation-inductively coupled plasma-mass spectrometry: evidence for mass load induced matrix effects in the ICP during ablation of silicate glass. *Journal of Analytical Atomic Spectrometry* **11**, 899–904.

Lorand, J. P., Alard, O., Luguet, A. & Keays, R. R. (2003). Sulfur and selenium systematics of the subcontinental lithospheric mantle: Inferences from the Massif Central xenolith suite (France). *Geochimica et Cosmochimica Acta* **67**, 4137–4151.

Loucks, R. R. & Mavrogenes, J. A. (1999). Gold Solubility in Supercritical Hydrothermal Brines Measured in Synthetic Fluid Inclusions. *Science* **284**, 2159–2163.

Macpherson, C. G., Hilton, D. R., Mattey, D. P. & Sinton, J. M. (2000). Evidence for an ^{18}O-depleted mantle plume from contrasting $^{18}O/^{16}O$ ratios of back-arc lavas from the Manus Basin and Mariana Trough. *Earth and Planetary Science Letters* **176**, 171–183.

Maier, W. D., Barnes, S.-J., Gartz, V. & Andrews, G. (2003). Pt–Pd reefs in magnetitites of the Stella layered intrusion, South Africa: A world of new exploration opportunities for platinum group elements. *Geology* **31**, 885–888.

Mallmann, G. & O'Neill, H. S. C. (2007). The effect of oxygen fugacity on the partitioning of Re between crystals and silicate melt during mantle melting. *Geochimica et Cosmochimica Acta* **71**, 2837–2857.

Mathez, E. A. (1976). Sulfur solubility and magmatic sulfides in submarine basalt glass. *Journal of Geophysical Research* **81**, 4269–4275.

Mavrogenes, J. A., Jenner, F. E. & Arculus, R. J. (2008). Magnetite fractionation of 'chalcophile' elements, American Geophysical Union, Fall Meeting, San Francisco, CA, USA, V33C-2229.

Melson, W. G., O'Hearn, T. & Jarosewich, E. (2002). A data brief on the Smithsonian Abyssal Volcanic Glass Data File. *Geochemistry, Geophysics, Geosystems* **3**, 1–11.

Métrich, N. & Clocchiatti, R. (1996). Sulfur abundance and its speciation in oxidised alkaline melts. *Geochimica et Cosmochimica Acta* **60**, 4151–4160.

Métrich, N., Schiano, P., Clocchiatti, R. & Maury, R. C. (1999). Transfer of sulfur in subduction settings: an example from Batan Island (Luzon volcanic arc, Philippines). *Earth and Planetary Science Letters* **167**, 1–14.

Métrich, N., Berry, A. J., O'Neill, H. S. C. & Susini, J. (2009). The oxidation state of sulfur in synthetic and natural glasses determined by X-ray absorption spectroscopy. *Geochimica et Cosmochimica Acta* **73**, 2382–2399.

Moss, R. & Scott, S. D. (2001). Gold content of eastern Manus Basin volcanic rocks: implications for enrichment in associated hydrothermal precipitates. *Economic Geology* **96**, 91–107.

Mungall, J. (2002). Roasting the mantle: Slab melting and the genesis of major Au and Au-rich Cu deposits. *Geology* **30**, 915–918.

Mysen, B. O. (1992). Iron and phosphorus in calcium silicate quenched melts. *Chemical Geology* **98**, 175–202.

Nebel, O., Morel, M. L. A. & Vroon, P. Z. (2009). Isotope dilution analyses of Lu, Hf, Zr, Ta and W, and Hf-isotope compositions of NIST SRM-610 and SRM-612 glass wafers. *Geostandards and Geoanalytical Techniques* **33**, 487–499.

Nilsson, K. & Peach, C. L. (1993). Sulfur speciation, oxidation state, and sulfur concentration in back-arc magmas. *Geochimica et Cosmochimica Acta* **57**, 3807–3813.

O'Neill, H. S. C. & Mavrogenes, J. A. (2002). The sulfide capacity and the sulfur content at sulfide saturation of silicate melts at 1400°C and 1 bar. *Journal of Petrology* **43**, 1049–1087.

Palme, H. & O'Neill, H. S. C. (2004). Cosmochemical estimates of mantle composition. In: Carlson, R. W. (ed.) *The Mantle and Core. Treatise on Geochemistry*. In: Holland, H. D. & Turekian, K. K. (eds), *Volume 2*, Elsevier, Oxford, pp. 1–38.

Parat, F. & Holtz, F. (2004). Sulfur partitioning between apatite and melt and effect of sulfur on apatite solubility at oxidizing conditions. *Contributions to Mineralogy and Petrology* **147**, 201–212.

Park, S.-H., Lee, S.-M., Kamenov, G. D. & Kwon, S.-T. (2010). Tracing the origin of subduction components beneath the south east rift in the Manus Basin, Papua New Guinea. *Chemical Geology* **30**, 339–349.

Peach, C. L., Mathez, E. A. & Keays, R. R. (1990). Sulfide melt–silicate melt distribution coefficients for noble metals and other chalcophile elements as deduced from MORB: Implications for partial melting. *Geochimica et Cosmochimica Acta* **54**, 3379–3389.

Pearce, J. A., Stern, R. C., Bloomer, S. H. & Fryer, P. (2005). Geochemical mapping of the Mariana arc–basin system: Implications for the nature and distribution of subduction components. *Geochemistry, Geophysics, Geosystems* **6**, doi:10.1029/2004GC000895.

Ripley, E. M., Brophy, J. G. & Chusi, L. (2002). Copper solubility in a basaltic melt and sulfide liquid/silicate melt partition coefficients of Cu and Fe. *Geochimica et Cosmochimica Acta* **66**, 2791–2800.

Rose-Weston, L., Brenan, J. M., Fei, Y. W., Secco, R. A. & Frost, D. J. (2009). Effect of pressure, temperature, and oxygen fugacity on the metal–silicate partitioning of Te, Se, and S: Implications for earth differentiation. *Geochimica et Cosmochimica Acta* **73**, 4598–4615.

Rudnick, R. L. & Gao, S. (2008). Composition of the continental crust. In: Rudnick, R. L. (ed.) *The Crust. Treatise on Geochemistry*. In: Holland, H. D. & Turekian, K. K. (eds), *Volume 3*, Elsevier, Oxford, pp. 1–56.

Sha, L.-K. (2000). Whitlockite solubility in silicate melts: some insights into lunar and planetary evolution. *Geochimica et Cosmochimica Acta* **64**, 3217–3236.

Shaw, D. M., Hilton, D. R., Macpherson, C. G. & Sinton, J. M. (2001). Nucleogenic neon in high $^{3}He/^{4}He$ lavas from the Manus back-arc basin : a new perspective on He–Ne decoupling. *Earth and Planetary Science Letters* **194**, 53–66.

Sillitoe, R. H. (2010). Porphyry copper systems. *Economic Geology* **105**, 3–41.

Sinton, J. M., Ford, L. L., Chappell, B. & McCulloch, M. T. (2003). Magma genesis and mantle heterogeneity in the Manus back-arc basin, Papua New Guinea. *Journal of Petrology* **44**, 159–195.

Stolper, E. & Newman, S. (1994). The role of water in the petrogenesis of Mariana trough magmas. *Earth and Planetary Science Letters* **121**, 293–325.

Sun, W., Arculus, R. J., Bennett, V. C., Eggins, S. M. & Binns, R. A. (2003). Evidence for rhenium enrichment in the mantle wedge from submarine arc-like volcanic glasses (Papua New Guinea). *Geology (Boulder)* **31**, 845–848.

Sun, W., Arculus, R. J., Kamenetsky, V. S. & Binns, R. A. (2004). Release of gold-bearing fluids in convergent margin magmas prompted by magnetite crystallization. *Nature* **431**, 975–978.

Sun, W. D., Binns, R. A., Fan, A. C., Kamenetsky, V. S., Wysoczanski, R., Wei, G. J., Hu, Y. H. & Arculus, R. J. (2007). Chlorine in submarine volcanic glasses from the eastern Manus basin. *Geochimica et Cosmochimica Acta* **71**, 1542–1552.

Sylvester, P. & Eggins, S. M. (1997). Analysis of Re, Au, Pd, Pt and Rh in NIST glass certified reference materials and natural basalt glasses by laser ablation ICP-MS. *Journal of Geostandards and Geoanalysis* **21**, 215–229.

Thy, P. & Lofgren, G. E. (1994). Experimental constraints on the low-pressure evolution of transitional and mildly alkalic basalts: the effect of Fe–Ti oxide minerals and the origin of basaltic andesites. *Contributions to Mineralogy and Petrology* **116**, 340–351.

Tollari, N., Toplis, M. J. & Barnes, S.-J. (2006). Predicting phosphate saturation in silicate magmas: An experimental study of the effects of melt composition and temperature. *Geochimica et Cosmochimica Acta* **70**, 1518–1536.

Toplis, M. J., Dingwell, D. B. & Libourel, G. (1994*a*). The effect of phosphorus on the iron redox ratio, viscosity, and density of an evolved ferrobasalt. *Contributions to Mineralogy and Petrology* **117**, 293–304.

Toplis, M. J., Libourel, G. & Carroll, M. R. (1994*b*). The role of phosphorus in crystallisation processes of basalt: An experimental study. *Geochimica et Cosmochimica Acta* **58**, 797–810.

Vogel, T. A., Cambray, F. W. & Constenius, K. N. (2001). Origin and emplacement of igneous rocks in the central Wasatch Mountains, Utah. *Rocky Mountains Geology* **36**, 119–162.

Watson, E. B. (1979). Apatite saturation in basic to intermediate magmas. *Geophysical Research Letters* **6**, 937–940.

Yamamoto, M. (1976). Fractionation of sulfur isotopes and selenium between coexisting sulfide minerals from the Besshi deposit, Central Shikoku, Japan. *Mineralium Deposita* **11**, 197–209.

Yi, W., Halliday, A. N., Alt, J. C., Lee, D.-C., Rehkämper, M., Garcia, M. O., Langmuir, C. H. & Su, Y. (2003). Cadmium, indium, tin, tellurium, and sulfur in oceanic basalts: Implications for chalcophile element fractionation in the Earth. *Journal of Geophysical Research* **105**, 18927–18948.

Zajacz, Z. & Halter, W. (2009). Copper transport by high temperature, sulfur-rich magmatic vapour; Evidence from silicate melt and vapour inclusions in a basaltic andesite from Villarrica volcano (Chile). *Earth and Planetary Science Letters* **282**, 115–121.